124

BioRadiations

A Resource for Life Science Research

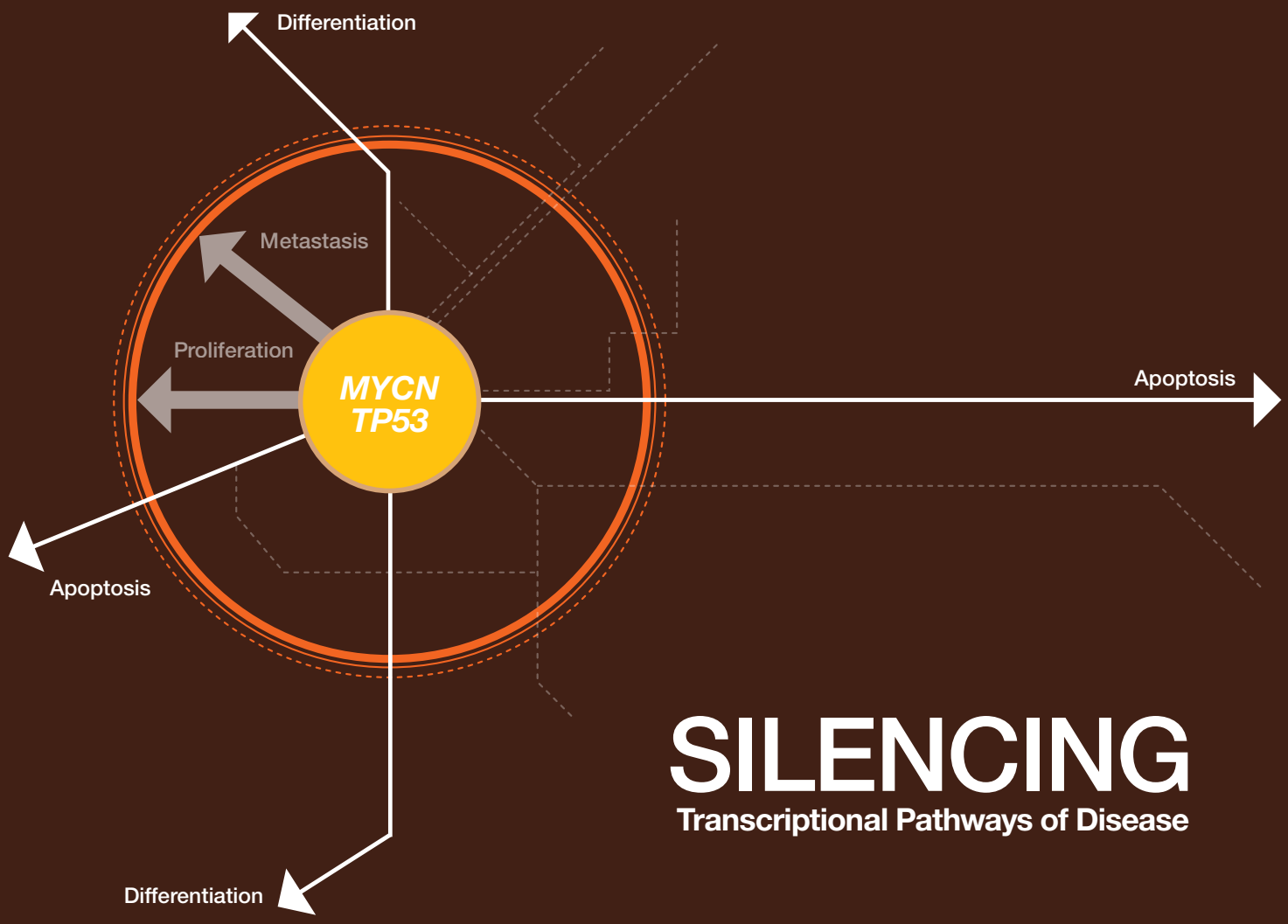

SILENCING

Transcriptional Pathways of Disease

In this issue:

BIO-RAD

My Tetra Is . . . Leakproof

The Mini-Protean® Tetra cell winged locking mechanism locks out leaks.

The Mini-PROTEAN Tetra systems for mini vertical gel electrophoresis feature an innovative locking mechanism that eliminates leakage issues commonly associated with gel electrophoresis. The patented* design makes it easy to lock handcast or precast gels into the electrophoresis module, ensuring leakproof operation and accurate experimental data. Designed to run as many as four SDS-PAGE gels simultaneously, the Mini-PROTEAN Tetra systems offer high throughput and a unique design to meet all your electrophoresis needs.

Key Features

- Patented locking system to eliminate leaks
- Capacity to run up to 4 mini SDS-PAGE gels
- Easy conversion from electrophoresis cell to blotting apparatus
- Error-proof design to ensure correct polarity and orientation

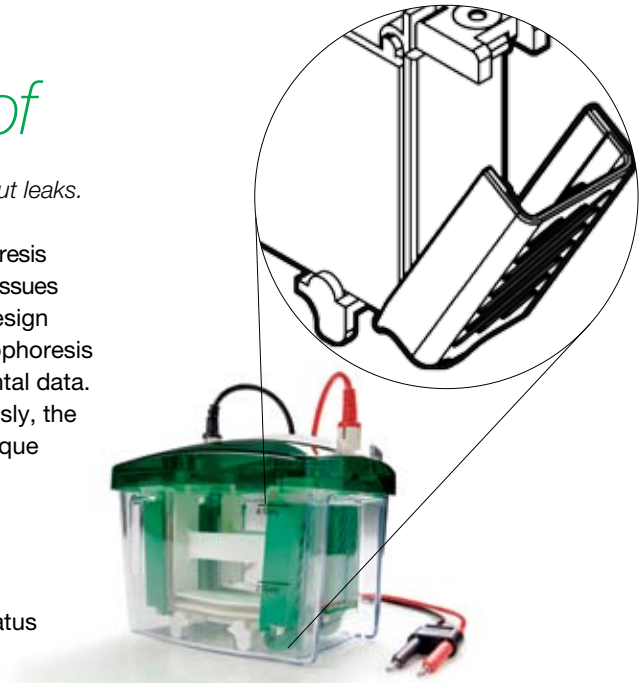

Reliable and easy to use.

* U.S. patent 6,436,262.

To find your local sales office, visit **www.bio-rad.com/contact/**
In the U.S., call toll free at 1-800-4BIORAD (1-800-424-6723)

Visit us on the Web at **discover.bio-rad.com**

BIO-RAD

BIO-RAD SUBSIDIARY TELEPHONE NUMBERS

Australia 61-2-9914-2800
Austria 43-1-877-89-01
Belgium 32-9-385-55-11
Brazil 55-21-3237-9400
Canada 905-364-3435
China 86-21-6426-0808
Czech Republic 420-241-430-532
Denmark 45-44-52-10-00
Finland 358-9-804-22-00
France 33-1-47-95-69-65
Germany 49-89-31884-0
Greece 30-210-777-4396
Hong Kong 852-2-789-3300
Hungary 36-1-455-8800
India 91-124-402-9300
Israel 03-963-6050
Italy 39-02-216091
Japan 81-3-6361-7000
Korea 82-2-3473-4460
Mexico 52-555-488-7670
The Netherlands 31-318-540666
New Zealand 0508-805-500
Norway 47-23-38-41-30
Poland 48-22-331-99-99
Portugal 351-21-472-7700
Russia 7-495-721-14-04
Singapore 65-6415-3188
South Africa 27-861-246-723
Spain 34-91-590-5200
Sweden 46-8-555-12700
Switzerland 41-61-717-9555
Taiwan 88-62-2578-7189
Thailand 662-651-8311
United Kingdom 44-20-8328-2000
USA Toll free 1-800-4BIORAD (1-800-424-6723)

discover.bio-rad.com

On the cover:
Conceptual illustration by Joann Ma

BioRadiations magazine is published by Bio-Rad Laboratories, Inc.
2000 Alfred Nobel Drive
Hercules, CA 94547 USA

If you have comments or suggestions regarding BioRadiations, please e-mail us at **bioradiations@bio-rad.com**

BioRadiations

issue 124, 2008

TO OUR READERS

One of the greatest challenges facing researchers studying the genetic components of disease, is discovering methodologies for silencing detrimental transcriptional pathways while preserving those that are beneficial. At Ghent University in Belgium, researchers are working to advance understanding how hyperactivity of the *MYCN* oncogene and low frequency of *TP53* mutations at diagnosis correlate to the most fatal forms of neuroblastoma. Using an optimized rt-qPCR workflow and integrating highly specific siRNA-based techniques, these researchers have developed gene knockdown models with more relevant silencing. Their ultimate goal is to completely unravel the *MYCN* transcriptional web, enabling therapeutic methods that interfere with the oncogenetic signaling pathways of *MYCN*, and leave the beneficial pathways unaltered. It is hoped that success in these efforts will significantly reduce mortality from this very deadly form of childhood cancer.

COVER STORY

DEPARTMENTS

TECHNICAL REPORTS

Legal Notices — See page 32.

Bio-Plex® Suspension Array System: New Assays and Updated Software

The Bio-Plex suspension array system can simultaneously measure multiple biomarkers in a single assay. Bio-Rad introduces three new panels of immunoassays to its line of Bio-Plex Pro™ assays, and introduces Bio-Plex Manager™ software, version 5.0.

Latest Bio-Plex Pro Assay Panels

Magnetic bead-based Bio-Plex Pro assays offer the option of using either magnetic separation or vacuum filtration during processing.

Bio-Plex Pro human diabetes assay panel — allows detection of 14 human diabetes and obesity biomarkers. Available in one 12-plex panel and two singleplex kits.

Bio-Plex Pro human acute phase assay panel — allows detection of 9 human acute phase response biomarkers. Available as 5-plex and 4-plex panel kits.

Bio-Plex Pro human angiogenesis assay panel — allows detection of 9 human angiogenesis biomarkers. Available as a 9-plex panel kit.

Available Targets

Human Diabetes	Human Acute Phase	Human Angiogenesis
Adiponectin	α-2-macroglobulin	Angiopoietin-2
Adipsin	CRP	Follistatin
C-peptide	Ferritin	G-CSF
Ghrelin	Fibrinogen	HGF
GIP	Haptoglobin	IL-8
GLP-1	Procalcitonin	Leptin
Glucagon	SAA	PDGF-BB
IL-6	SAP	PECAM-1
Insulin	Tissue plasminogen activator	VEGF
Leptin		
PAI-1		
Resistin		
TNF-α		
Visfatin		

Features of all kits include:

- Validation in serum, plasma, and tissue culture samples
- Premixed assays for convenience and reproducibility
- Magnetic- or vacuum-based separation
- Contain both standards and controls
- Include targets unique to the xMAP platform

Bio-Plex Manager Software, Version 5.0

This latest software version provides:

- Tabulating and graphing functions — visualize results and generate data figures faster
- Statistical analysis and data normalization functions for normalization across different plates, samples, or experiments
- Programmable wash, preparation, and shutdown steps for reading of assays unattended

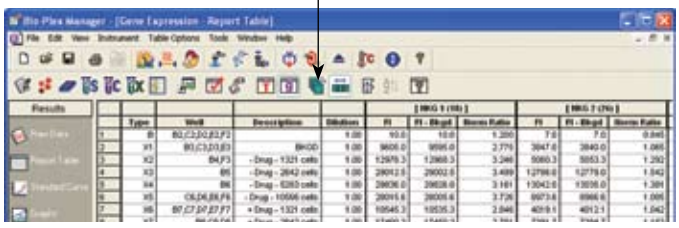

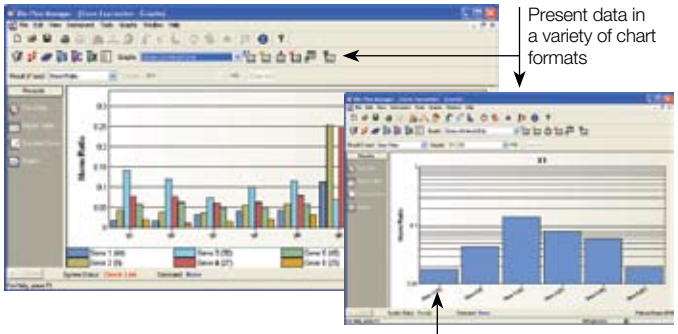

For available assay configurations, complete software information, and ordering information, go to **www.bio-rad.com/bio-plex/**

ProteoMiner™ Protein Enrichment Kits

ProteoMiner protein enrichment technology is a novel sample preparation tool for reducing the dynamic range of protein concentrations in complex biological samples. The presence of high-abundance proteins in biological samples (for example, albumin and IgG in serum or plasma) makes the detection of low-abundance proteins extremely challenging. ProteoMiner technology overcomes this challenge by:

- Utilizing a combinatorial library of hexapeptides rather than immunodepletion to decrease high-abundance proteins — allows use with a variety of sample types and prevents codepletion of low-abundance proteins
- Enriching and concentrating low-abundance proteins that cannot be detected through traditional methods

ProteoMiner kits enable the enrichment and detection of low-abundance proteins for one- or two-dimensional gel electrophoresis, chromatography, surface-enhanced laser desorption/ionization (SELDI), or another mass spectrometry technique.

For more information, go to **www.bio-rad.com/proteominer/**

Untreated serum

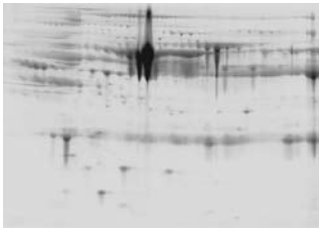

Treated serum

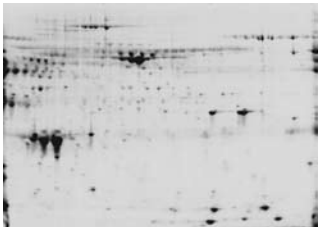

Reduction of high-abundance proteins improves detection and resolution of proteins. Top, untreated serum; bottom, serum treated using the ProteoMiner protein enrichment kit.

Ordering Information

Catalog #	Description
163-3000	ProteoMiner Protein Enrichment Kit, 10 preps, includes 10 spin columns, wash buffer, elution reagents, collection tubes
163-3001	ProteoMiner Introductory Kit, 2 preps, includes 2 spin columns, wash buffer, elution reagents, collection tubes
163-3002	ProteoMiner Sequential Elution Kit, 10 preps, includes 10 spin columns, wash buffer, 4 sequential elution reagents, collection tubes
163-3003	ProteoMiner Sequential Elution Reagents, includes reagents only (columns not included), to be used with 163-3000

Profinity eXact™ Fusion-Tag System

The Profinity eXact fusion-tag system is the latest complement to the Bio-Rad line of affinity purification tools for recombinant tag purification. This integrated set of products allows expression, detection, purification, and on-column cleavage of fusion-tagged proteins, without the addition of protease. Cleavage occurs in as little as 30 minutes, a significant time savings compared to traditional methods. A highly purified, recombinant protein containing only its native amino acid sequence is generated in a single step and in a fraction of the time of other methods. The result is true, single-step purification without cleavage enzymes, incubation times, or removal of reagents.

Ordering Information

Catalog #	Description
156-3000	Profinity eXact Cloning and Expression Starter Kit
156-3001	Profinity eXact pPAL7 RIC-Ready Expression Vector Kit
156-3002	Profinity eXact pPAL7 Supercoiled Expression Vector Kit
156-3003	BL21(DE3) Chemi-Competent Expression Cells
156-3004	Profinity eXact Antibody Reagent
156-3005	Profinity eXact Purification Resin, 10 ml
156-3006	Profinity eXact Mini Spin Purification Starter Kit
156-3007	Profinity eXact Mini Spin Columns
156-3008	Profinity eXact Expression and Purification Starter Kit
732-4646	Bio-Scale Mini Profinity eXact Cartridges, 2 x 1 ml
732-4647	Bio-Scale Mini Profinity eXact Cartridges, 4 x 1 ml
732-4648	Bio-Scale Mini Profinity eXact Cartridges, 1 x 5 ml

1000-Series Thermal Cyclers

The new Bio-Rad 1000-series thermal cyclers offer superior performance in a flexible and fully modular platform. Choose the full-featured C1000™ cycler, the basic S1000™ cycler, or a combination of both — there are multiple configuration options.

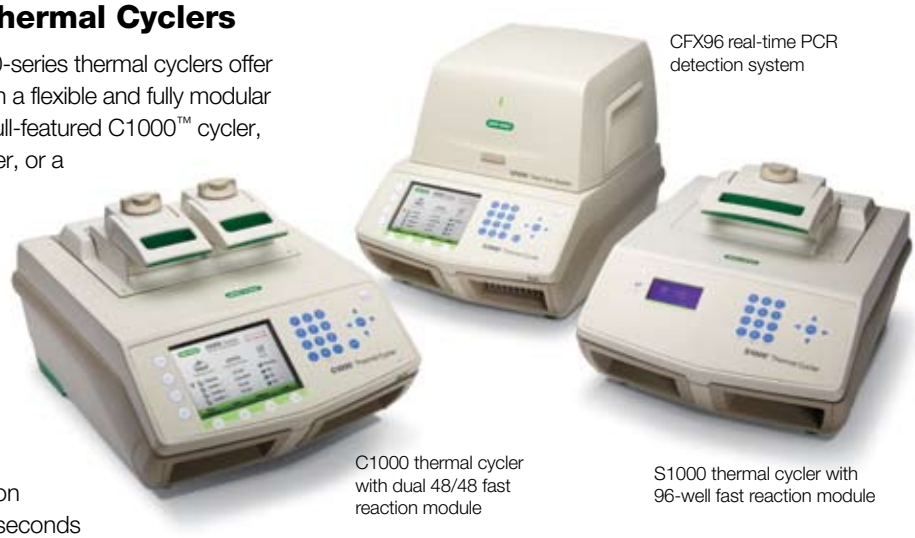

CFX96 real-time PCR detection system

C1000 thermal cycler with dual 48/48 fast reaction module

S1000 thermal cycler with 96-well fast reaction module

Interchangeable Reaction Modules

Accommodate different throughput needs with easily interchangeable reaction modules that swap in seconds without requiring tools. The four reaction module formats include a gradient-enabled 96-well fast module, a gradient-enabled dual 48-well fast module that allows two independently controlled protocols to be run side by side in a single bay, a 384-well module for high throughput, and the CFX96™ optical reaction module with five-target real-time PCR capabilities (see page 5). Each PCR reaction module has a fully adjustable lid that supports a wide range of sealers and vessels, including low-profile and standard-height plates.

Multiple Configuration Options

C1000 and S1000 thermal cyclers are available in two configurations: as stand-alone units or connected via USB cables for operation as a multi-bay cycler. The following options are available for multi-bay cycler configurations:

- Connect a C1000 thermal cycler with up to three S1000 thermal cyclers for four-bay cycling
- Add a PC with C1000 Manager™ desktop software for control of up to 32 cyclers simultaneously

Performance

The overall run time of a PCR reaction depends on protocol design, enzyme type, and the thermal capabilities of the thermal cycler. The 1000-series thermal cyclers deliver premium thermal performance for reproducible results and fast run times. The time to reach target temperature, which depends on the average ramp rate and the settling time (the time it takes to reach thermal uniformity), is the key factor determining how fast a thermal cycler can run a given PCR protocol. Average ramp rate is a better indicator of a cycler's capabilities than maximum ramp rate, because the latter is generally not maintained throughout a temperature step. The average ramp rate of 1000-series cyclers, combined with a 10 second settling time, allows fast run times while maintaining excellent thermal accuracy and uniformity.

Ordering Information

Catalog #	Description
C1000 Thermal Cycler	
185-1048	C1000 Thermal Cycler With Dual 48/48 Fast Reaction Module
185-1096	C1000 Thermal Cycler With 96-Well Fast Reaction Module
185-1384	C1000 Thermal Cycler With 384-Well Reaction Module
S1000 Thermal Cycler	
185-2048	S1000 Thermal Cycler With Dual 48/48 Fast Reaction Module
185-2096	S1000 Thermal Cycler With 96-Well Fast Reaction Module
185-2384	S1000 Thermal Cycler With 384-Well Reaction Module
CFX96 Real-Time Detection System	
185-5096	CFX96 Real-Time PCR Detection System, includes C1000 thermal cycler chassis, CFX96 optical reaction module, CFX Manager software, communication cable, power cord, reagent and consumable samples, instructions

CFX96™ Real-Time PCR Detection System

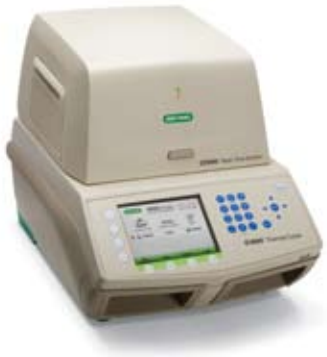

The CFX96 optical reaction module converts a C1000™ thermal cycler into a powerful and precise real-time PCR detection system. This six-channel system's solid-state optical technology (filtered LEDs and photodiodes) maximizes fluorescent detection of dyes in specific channels, providing precise quantitation and target discrimination. At every position and with every scan, the optics shuttle is reproducibly centered above each well, so the light path is always optimal and there is no need to sacrifice data collection to normalize a passive reference. Features include:

- Data collection from all wells during acquisition — enter/edit plate information before, during, or after the run
- Multiple data acquisition modes — tailor the run to suit your application (including 1-color fast scan mode for SYBR® Green users)
- CFX Manager™ software — use advanced analysis tools for performing normalized gene expression with multiple reference genes and individual reaction efficiencies
- Expansion capability — run up to 4 instruments from 1 computer
- E-mail notification — program software to send an e-mail with an attached data file upon run completion

Ordering Information

Catalog#	Description
184-5096	CFX96 Optical Reaction Module, includes CFX96 optics shuttle, CFX Manager software, communication cable, reagent and consumable samples, instructions
185-5096	CFX96 Real-Time PCR Detection System, includes C1000 thermal cycler chassis, CFX96 optical reaction module, CFX Manager software, communication cable, power cord, reagent and consumable samples, instructions

siLentMer™ Validated siRNAs With Validated qPCR Primer Pairs

Now, every siLentMer validated siRNA duplex is packaged with the validated qPCR primer pairs that were used for the siRNA validation studies. This enables you to quickly study knockdown efficiency for your target of interest. Examples of qPCR validation of siLentMer siRNA knockdown efficiency are shown below.

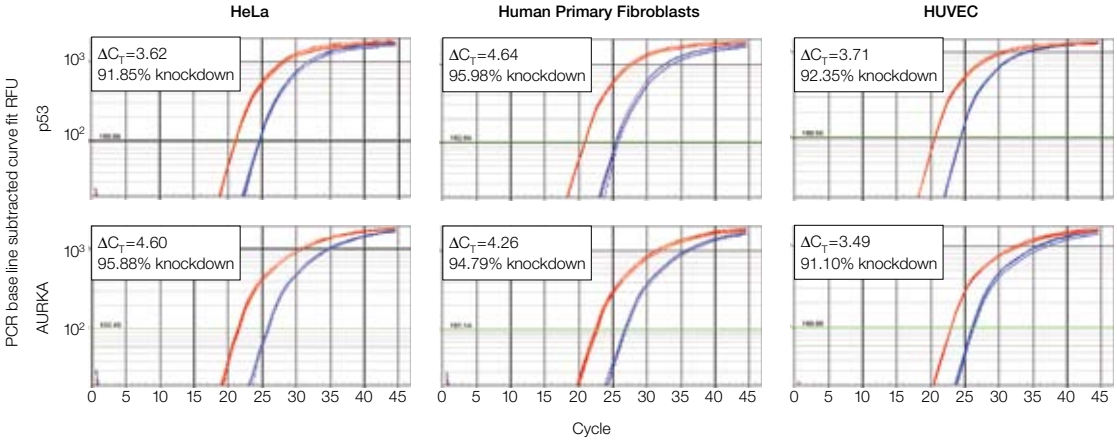

siLentMer siRNAs produce effective gene silencing with greater than 90% knockdown of multiple genes in multiple cell lines. Silencing of either the tumor suppressor gene (*TP53*) or aurora kinase A gene (*AURKA/STK15/BTAK*) in HeLa cells, human primary fibroblasts, and human umbilical vein endothelial cells (HUVEC) is demonstrated. The RT-qPCR traces, generated using validated qPCR primer pairs, show gene expression in cells transfected with a nonsilencing siRNA (—), or an siRNA targeting either *TP53* or *AURKA* mRNAs (—). All cells were transfected using siLentFect™ lipid transfection reagent, then exposed to siRNA (HeLa, 5 nM siRNA; human primary fibroblasts and HUVEC cells, 10 nM siRNA). RNA samples were collected 24 hr posttransfection and knockdown efficiency was measured by RT-qPCR using the coordinated validated qPCR primer pairs for the target gene.

For ordering information, go to **www.bio-rad.com/rnai/**

siLentMer™ Validated siRNAs With Validated qPCR Primer Pairs

The Bio-Rad line of siLentMer validated Dicer-substrate siRNA duplexes is continuously growing; currently available gene targets are listed in the table below. Two duplexes per target are offered to confirm that any biological effects observed in the experiments are specifically due to loss of the targeted gene. For more information, go to **www.bio-rad.com/RNAi/**

Available Gene Targets

Human Gene Target	Accession #*	Catalog # Duplex 1	Catalog # Duplex 2
Reference/Housekeeping Genes			
β-Actin	NM_001101	179-0104	179-0204
Cyclophilin A	NM_021130	179-0103	179-0203
GAPDH	NM_002046	179-0100	179-0200
GFP (jellyfish)	M62653	179-0106	—
Genes of Research Interest			
ABCB1	NM_000927	179-0182	179-0282
ABL1	NM_005157	179-0135	179-0235
ACVR1	NM_001105	179-0164	179-0264
ACVR2B	NM_001106	179-0192	179-0292
ADCK1	NM_020421	179-0165	179-0265
ADCK2	NM_052853	179-0176	179-0276
AIFM1	NM_004208	179-0151	179-0251
AKT1	NM_001014431	179-0118	179-0218
AKT2	NM_001626	179-0155	179-0255
APC	NM_000038	179-0110	179-0210
ATF2	NM_001880	179-0130	179-0230
AURKA	NM_003600	179-0185	179-0285
B2M	NM_004048	179-0109	179-0209
BAX	NM_004324	179-0124	179-0224
BCR	NM_004327	179-0126	179-0226
BRCA1	NM_007294	179-0127	179-0227
CAMK1	NM_003656	179-0190	179-0290
CASP1	NM_001223	179-0148	179-0248
CASP2	NM_032982	179-0140	179-0240
CASP4	NM_001225	179-0161	179-0261
CASP7	NM_001227	179-0139	179-0239
CCND1	NM_053056	179-0186	179-0286
CCNE1	NM_001238	179-0194	179-0294
CDC2 (CDK1)	NM_001786	179-0113	179-0213
CDC42BPA	NM_003607	179-0196	179-0296
CDK2	NM_001798	179-0114	179-0214
CDK4	NM_000075	179-0117	179-0217
CDK5	NM_004935	179-0120	179-0220
CDK7	NM_001799	179-0166	179-0266
CDKN1A	NM_000389	179-0158	179-0258
CHEK1	NM_001274	179-0189	179-0289
CHUK	NM_001278	179-0122	179-0222
COPB1	NM_016451	179-0301	179-0401
CREB1	NM_004379	179-0199	179-0299
CSK	NM_004383	179-0152	179-0252
CTNNB1	NM_001904	179-0168	179-0268
E2F1	NM_005225	179-0145	179-0245
EGFR	NM_005228	179-0115	179-0215
ELK1	NM_005229	179-0131	179-0231
FYN	NM_002037	179-0144	179-0244
GSK3A	NM_019884	179-0116	179-0216
GSK3B	NM_002093	179-0159	179-0259
HDGF	NM_004494	179-0300	179-0400
HIPK1	NM_152696	179-0184	179-0284
HK1	NM_000188	179-0180	179-0280
IGF1R	NM_000875	179-0174	179-0274
IL1A	NM_000575	179-0195	179-0295

Available Gene Targets

Human Gene Target	Accession #*	Catalog # Duplex 1	Catalog # Duplex 2
Reference/Housekeeping Genes			
HPRT1	NM_000194	179-0101	179-0201
Lamin A/C	NM_005572	179-0102	179-0202
Luciferase (firefly)	X84846	179-0107	—
β-Tubulin	NM_178014	179-0105	—
Genes of Research Interest			
ILK	NM_001014794	179-0121	179-0221
IRAK1	NM_001025242	179-0160	179-0260
IRAK2	NM_001570	179-0175	179-0275
IRAK4	NM_016123	179-0183	179-0283
JAK1	NM_002227	179-0179	179-0279
LATS2	NM_014572	179-0198	179-0298
LIMK1	NM_002314	179-0169	179-0269
LIMK2	NM_001031801	179-0177	179-0277
LYN	NM_002350	179-0138	179-0238
MAP2K1	NM_002755	179-0125	179-0225
MAP2K4	NM_003010	179-0193	179-0293
MAP2K5	NM_002757	179-0197	179-0297
MAP3K3	NM_002401	179-0188	179-0288
MAPK1	NM_002745	179-0153	179-0253
MAPK3	NM_001040056	179-0146	179-0246
MAPK8	NM_002750	179-0123	179-0223
MAPKAPK2	NM_004759	179-0163	179-0263
MARK2	NM_004954	179-0142	179-0242
MDM2	NM_002392	179-0134	179-0234
MEN1	NM_000244	179-0141	179-0241
MET	NM_000245	179-0112	179-0212
MMP2	NM_004530	179-0149	179-0249
NF1	NM_000267	179-0171	179-0271
NFKB1	NM_003998	179-0154	179-0254
PDK1	NM_002610	179-0172	179-0272
PDK2	NM_002611	179-0156	179-0256
PDK3	NM_005391	179-0162	179-0262
PLK1	NM_005030	179-0119	179-0219
PPARA	NM_001001928	179-0178	179-0278
PTK2	NM_005607	179-0128	179-0228
RAF1	NM_002880	179-0137	179-0237
RB1	NM_000321	179-0132	179-0232
RBBP8	NM_002894	179-0302	179-0402
ROCK2	NM_004850	179-0167	179-0267
RXRA	NM_002957	179-0147	179-0247
SKI	NM_003036	179-0143	179-0243
STAT1	NM_007315	179-0129	179-0229
STAT3	NM_003150	179-0157	179-0257
TEC	NM_003215	179-0150	179-0250
TGFBR2	NM_001024847	179-0187	179-0287
TK1	NM_003258	179-0181	179-0281
TK2	NM_004614	179-0191	179-0291
TNFRSF1A	NM_001065	179-0173	179-0273
TP53	NM_000546	179-0111	179-0211
VEGFA	NM_001025366	179-0133	179-0233
WEE1	NM_003390	179-0170	179-0270
YES1	NM_005433	179-0136	179-0236

* National Center for Biotechnology Information (NCBI) accession number.

ProteOn™ XPR36 Protein Interaction Array System Receives 2007 Product of the Year Award

The ProteOn XPR36 protein interaction array system, a surface plasmon resonance (SPR) biosensor, was chosen by Frost & Sullivan as the 2007 U.S. Drug Discovery Technologies Product of the Year. Frost & Sullivan, a global growth consulting company, recognizes companies in a variety of regional and global markets for outstanding achievement and superior performance in areas such as leadership, technological innovation, customer service, and strategic product development.

According to Frost & Sullivan analyst Shankar Sellappan, PhD, the ProteOn XPR36 system was selected for the award because of its unique ability to monitor multiple cellular molecular interactions independently, which "assists in efforts to better understand the biological mechanisms that maintain normal cellular processes and that contribute to disease development and progression and assists in the development of drugs."

Factors considered by analysts in their evaluation of new products include:

- Significance of the product in its industry
- Competitive advantage of the product in its industry
- Innovation in terms of unique or revolutionary technology
- Acceptance in the marketplace
- Value-added services provided to customers
- Number of competitors with similar product(s)

The ProteOn XPR36 Protein Interaction Array System

The ProteOn XPR36 system is a unique 6 x 6 multichannel SPR platform that enables automated analysis of up to 36 biomolecular interactions in one experiment. Advantages of the ProteOn XPR36 system — high throughput, speed, kinetic response — are multiplied for research that involves large, broad, and complex studies, such as results from hybridoma screening and ranking data and results from the validation and characterization of small molecule-target interactions. In addition, multiplexed analysis using crisscross microfluidics, made possible by XPR™ technology, enables rapid generation of large amounts of complex data. Results are quickly ready for comparison, seamlessly integrated, and easily categorized.

The Power of One-Shot Kinetics™

Until recently, SPR experiments for the evaluation of kinetic rate constants could only be run sequentially. Following the immobilization of one ligand on the sensor chip surface, a single concentration of analyte was flowed over the ligand and the corresponding response was measured. The surface was then regenerated (analyte removed) to prepare the immobilized ligand for the next concentration of analyte. This sequence was repeated until a full analyte concentration series was collected.

The ProteOn XPR36 system uses a more powerful method, combining multiplexed SPR technology and a unique One-Shot Kinetics approach. Multiplexing improves the capabilities and workflow of traditional technology by enabling multiple quantitative protein binding experiments in parallel, so robust kinetic analysis of an analyte concentration series can be handled in one experiment. This one-shot approach generates a complete kinetic profile of a biomolecular interaction — without the need for regeneration — in one experiment, using a single sensor chip.

The ProteOn system can be used for a variety of drug discovery and life science research applications, including protein-protein interaction analyses, protein-drug target binding, antibody profiling, protein-interface mapping, and protein complex assembly and signaling cascades. This versatility and the parallel processing workflow allow more information to be generated from each experiment, which has the potential to accelerate understanding of cellular processes and the development of drugs.

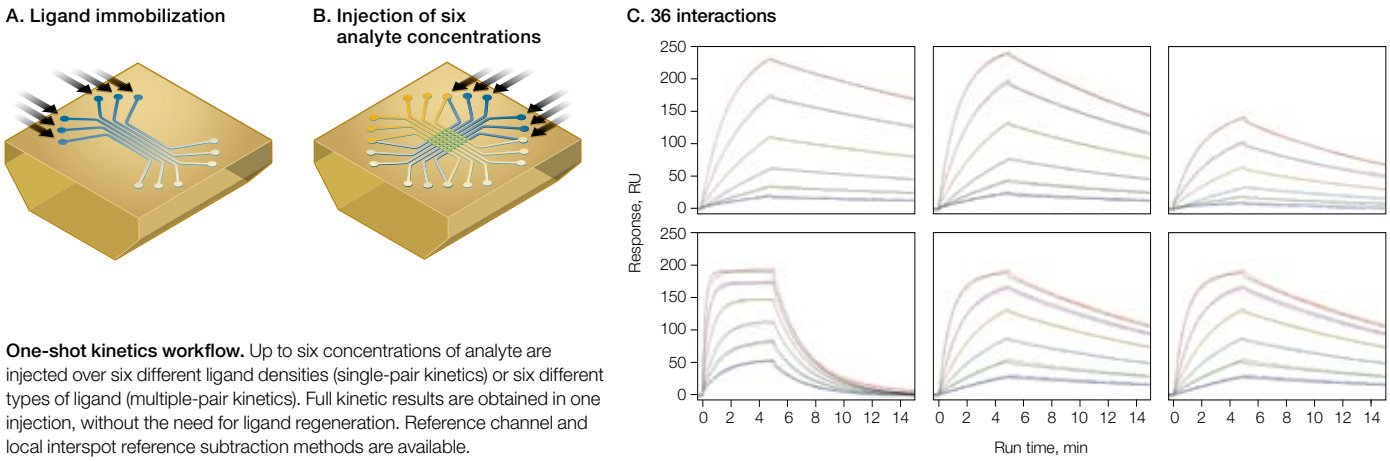

One-shot kinetics workflow. Up to six concentrations of analyte are injected over six different ligand densities (single-pair kinetics) or six different types of ligand (multiple-pair kinetics). Full kinetic results are obtained in one injection, without the need for ligand regeneration. Reference channel and local interspot reference subtraction methods are available.

Tips for Experion™ System Users: RNA Assays

RNA can be a temperamental molecule to work with and can cause countless hours of frustration. Difficulties are generally attributed to ubiquitous RNases — enzymes that catalyze the hydrolysis of RNA (Figure 1). Careful and consistent laboratory practices can help improve RNA assay results. Bio-Rad technical support specialists have developed the following tips to help overcome RNA assay problems when using the Experion automated electrophoresis system.

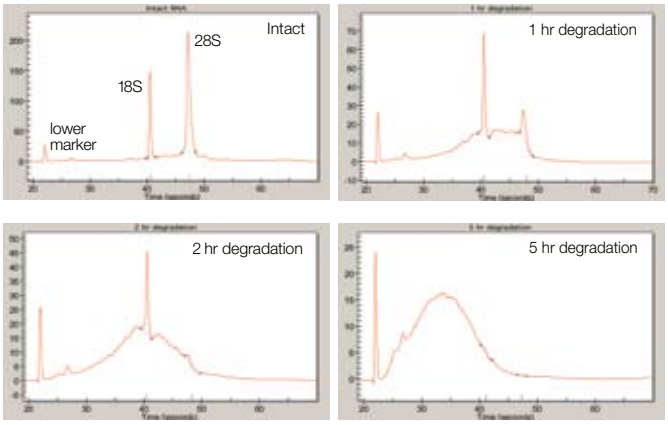

Fig. 1. Time course of degradation of liver carcinoma RNA. Samples of human liver carcinoma total RNA were incubated at 90°C in TE buffer in 1 hr increments from 0 to 7 hr. Aliquots (50 ng) were then separated with the Experion RNA StdSens analysis kit. Electropherograms of samples collected at selected time points are shown.

Analyze RNA ladder quality — first, perform a quick check of the ladder prior to analyzing results to ensure the run was successful and the results were unaffected by RNase contamination. As the basis for any sizing and quantitation that occurs on the chip, it is essential to confirm that a good RNA ladder profile has been created. To do this, verify that the RNA ladder pattern is correct and that all bands in the virtual gel have been correctly labeled from 50 to 6,000 bp. Electropherogams demonstrating good and poor ladder profiles are shown in Figure 2.

Clean electrodes — if ladder quality is poor, clean the electrodes in the electrophoresis station using one of the two methods outlined in the system manual. The milder cleaning method involves using the cleaning chips (supplied with RNA chips) to clean before and after each run. The deep cleaning method is performed using Experion electrode cleaner and a special lint-free swab, and should be done: when you suspect contamination, when switching between RNA and protein assays on the same system, as part of regular maintenance, and prior to any critical experiment.

Minimize contaminants — separate reagents and pipets from other general supplies, use disposable items whenever possible,

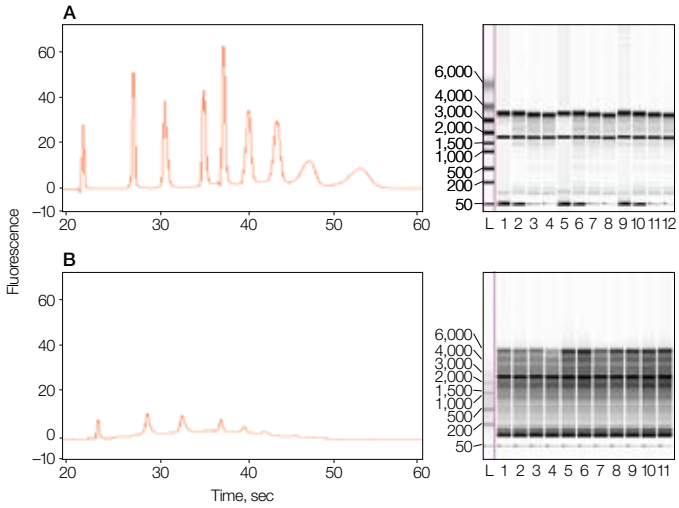

Fig. 2. Good and poor ladder profiles. A good ladder profile (**A**) shows a clearly identified lower marker (LM) and eight peaks that gradually get smaller over time. A poor ladder profile (**B**), shows poor peak resolution from the baseline, particularly for the last two peaks (results commonly seen from a degraded ladder). Note that in the "L" lane, the 6,000 bp marker of the ladder has not been identified.

use nuclease-free tips and tubes, use barrier tips, wear a face mask when preparing samples and chips, and wear gloves. If typical decontaminants do not clean surfaces effectively, use 1 M NaOH or HCl solution.

Develop standard procedures — aliquot single-use amounts of ladder into nuclease-free tubes (one for each chip); quickly snap-freeze aliquots on dry ice and do not reuse or refreeze them. Use the ladder quickly after thawing; thawing for extended periods after heating causes the ladder to renature, resulting in broad peaks. Inadequate heating also causes broad peaks (check the heating block if broad peaks are a recurring problem). RNA assays are sensitive to contaminants, salts, and detergents, so ensure samples are resuspended in DEPC-treated water (StdSens analysis kit and HighSens analysis kit) or TE buffer (StdSens kit only). The stain used in the Experion RNA analysis kits is sensitive to light; if damaged, the levels of fluorescence may be diminished and some peaks may go undetected. To protect the stain from photobleaching, wrap the tube in aluminum foil.

Determine concentration range of the sample load — desired ranges are: for detection only, 5–500 ng/µl (StdSens chip) and 100–5,000 pg/µl (HighSens chip), and for quantitation, 25–500 ng/µl (StdSens chip) and 500–5,000 pg/µl (HighSens chip). When the chip is over- or underloaded beyond the recommended ranges, data may no longer fall within the linear range and, therefore, cannot be accurately quantitated. To determine concentration, run a set of serial dilutions on the chip to find the optimal range.

— Katy McGirr, PhD, senior technical support consultant, Bio-Rad Laboratories

C1000™ Thermal Cycler: Unveiling the Protocol Autowriter

What Is the Protocol Autowriter and How Does It Save Time?

The protocol autowriter, a key innovation of the C1000 thermal cycler, automatically generates a customized temperature protocol with hot start, initial denaturation, and annealing and extension steps based on parameters you input as well as on standard PCR guidelines. It can create protocols that run at standard, fast, and even ultrafast speeds. The protocol autowriter is available on the C1000 thermal cycler and in C1000 Manager™ software, which runs on a PC.

How Does the Protocol Autowriter Work?

The protocol autowriter uses standard PCR guidelines that automatically generate cycling protocols with initial template denaturation and enzyme activation, followed by cycles of denaturation, annealing, and extension, and then final extension steps. Protocols are based on user-input parameters of target amplicon length, enzyme type, annealing temperature, and primer sequences. The protocol autowriter uses established PCR standards that reference data tables to produce the final suggested protocols. All protocols are either standard two- or three-step methods with a final extension step.

Protocols generated by the protocol autowriter at various speed settings (standard, fast, and ultrafast) may result in different product yields. In generating these protocols, the protocol autowriter may adjust the annealing temperature, reduce the total number of protocol steps, reduce the number of GOTO repeats, shorten hold times, or reduce the temperature differentials between steps.

The protocol autowriter can:

Autowrite a protocol — software will automatically suggest a temperature protocol based on user-input experimental parameters (amplicon length, annealing temperature, and enzyme type). An optional T_a (annealing temperature) calculator is also available. This suggested protocol may then be run or saved as is, or edited and saved as a standard temperature protocol.

Suggest temperature protocols with shorter run times — once initial parameters have been entered, choose a protocol "speed" for the total run time. The settings are standard, fast, and ultra-fast. The faster the protocol setting, the more chance that risk is introduced in terms of yield and successful amplification (particularly if difficult templates are involved).

Quickly program the C1000 cycler — a three-screen wizard permits very fast programming of new protocols and also helps users with little knowledge of PCR to write protocols.

Provide tools to further optimize a reaction — further optimization of reactions is possible by incorporating the gradient feature. Comparative reactions can even be run side-by-side on the dual 48/48 fast reaction module. Any change to the settings will result in a recalculation of the estimated run time, which will allow tailoring of run settings — maximizing the productivity of the cycler for a given experiment.

How Is the Protocol Autowriter Used?

1. Enter the amplicon length, polymerase, and primer T_m. If the primer T_m, is unknown, select the T_a calculator (F1) to calculate this value.

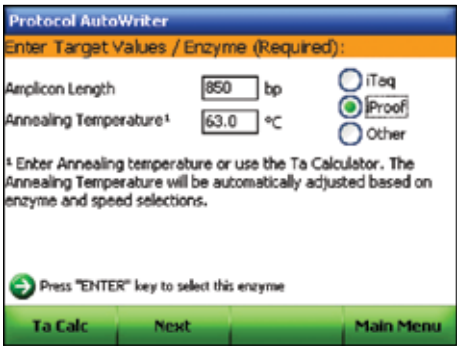

2. Select the protocol speed: standard, fast, or ultrafast.

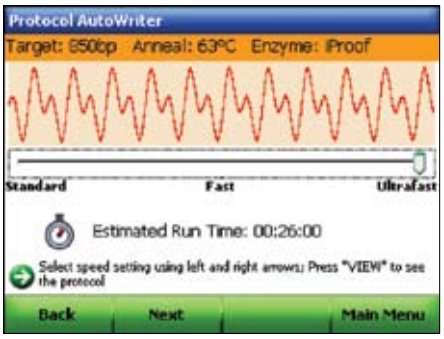

3. Edit, save, then run the suggested protocol.

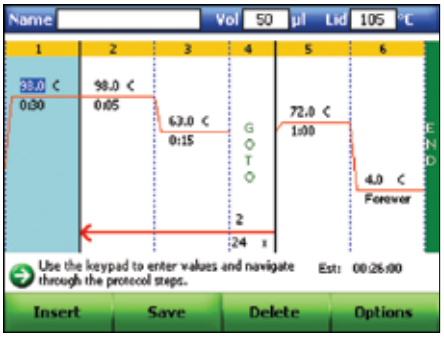

ProteoMiner™ Protein Enrichment System: Optimization of Sample and Bead Volumes

Introduction

Biological samples such as human plasma and serum are thought to contain valuable information for the discovery of biomarkers. However, the plasma proteome is extremely complex and has a wide protein dynamic range, factors that make the detection of low-abundance proteins nearly impossible (Anderson and Anderson 2002). No single analytical method is capable of resolving all plasma or serum proteins, and no detection method can cover more than 4 or 5 orders of magnitude. Therefore, most analytical methods for these sample types involve the immunodepletion of high-abundance proteins to reduce both the complexity and dynamic range of samples. Although immunodepletion is effective, it also has disadvantages and limitations: 1) the availability of antibodies against high-abundance proteins is limited, 2) available antibodies have a limited binding capacity, which in turn limits the amount of protein that can be loaded, and 3) there is a high probability for codepletion of low-abundance proteins.

To address the challenges of analyzing plasma and serum samples, and to mitigate the limitations of immunodepletion, Bio-Rad has developed the ProteoMiner protein enrichment system. The ProteoMiner system utilizes an extremely diverse combinatorial library of hexapeptides that are bound to beads. These hexapeptides act as unique protein binders to reduce sample complexity. Unlike immunodepletion, in which the capacity of the bound antibodies typically limits the sample volume to less than 100 µl, large sample volumes of 1 ml and more can be incubated with the hexapeptide beads. Binding of high-abundance proteins is limited by the bead capacity; therefore, proteins in high abundance quickly saturate their specific affinity ligands and cease binding. Excess unbound proteins are eventually washed away. In contrast, medium- and low-abundance proteins do not saturate their ligands and are therefore concentrated on the beads. When eluted, the sample is less complex, allowing detection of these medium- and low-abundance proteins by chromatography, gel electrophoresis, or mass spectrometry techniques, such as surface-enhanced laser desorption/ionization (SELDI).

The best results are achieved when sample and bead volumes are optimized to ensure coverage across the proteome, to reach an appropriate amount of saturation of ligands to reduce high-abundance proteins, and to enrich low-abundance proteins. The recommendation is to use 1 ml of plasma or serum (or ≥50 mg of protein) with 100 µl of beads (provided in each spin column in the ProteoMiner protein enrichment kit). However, due to samples with limited volume and low protein concentrations, it is often tempting to reduce either the sample or bead volume. In this study, we demonstrate the effects of reducing both the sample and bead volumes in an attempt to determine the optimal experimental conditions for the ProteoMiner protein enrichment kit.

Sample Preparation Using ProteoMiner Beads

In the ProteoMiner protein enrichment kit, beads (100 µl volume) are stored in spin columns in a 20% ethanol, 0.5% sodium azide solution. After centrifugation to remove the storage solution, ProteoMiner beads were washed with deionized water followed by phosphate buffered saline (PBS). Then 1 ml plasma (50 mg/ml) was applied to the column (10:1 sample-to-bead ratio) and, to ensure effective binding, the sample was slowly rotated with the ProteoMiner beads for 2 hr prior to washing with PBS buffer to remove the unbound proteins. To elute the bound proteins, the ProteoMiner beads were washed three times with 100 µl of acidic urea/CHAPS buffer (5% acetic acid, 8 M urea, 2% CHAPS), which is directly compatible with downstream SELDI and two-dimensional gel electrophoresis (2DGE). This protocol was repeated several times with different sample and bead volumes (Table 1).

Table 1. Sample and bead volumes tested with resulting spot count data from highlighted regions of 2-D gels (Figure 1).

Sample Volume, µl	Bead Volume, µl	Sample-to-Bead Ratio	Spot Count	Yield, mg
1,000	100	10:1	196	2.02
400	100	4:1	155	1.70
500	50	10:1	173	1.26
200	50	4:1	141	0.62

Gel Electrophoresis and Gel Image Analysis

For 2DGE experiments, 100 µg of each eluate was loaded onto an 11 cm ReadyStrip™ IPG strip, pH 5–8. Isoelectric focusing was performed at 250 V for 30 min followed by 8,000 V until 45,000 V-hr were reached. After transfer onto Criterion™ 8–16%

Tris-HCl gels, the second dimension was run for 1 hr at 200 V prior to staining with Flamingo™ fluorescent gel stain. Gels were imaged using the Molecular Imager® PharosFX™ system and analyzed with PDQuest™ 2-D analysis software, version 8.0.

SELDI Measurements

For this study, ProteinChip® CM10 arrays were used. The carboxymethyl weak cation exchange arrays were equilibrated twice with 5 µl of 100 mM sodium acetate buffer, pH 4. After equilibration, the liquid was removed from the ProteinChip arrays, and 0.5 µl of ProteoMiner bead-treated serum sample was mixed with 4.5 µl of 100 mM sodium acetate buffer, pH 4. After a 30 min incubation with shaking, each spot was washed three times with 5 µl of binding buffer for 5 min to eliminate unadsorbed proteins, followed by a quick rinse with deionized water. After air-drying, ProteinChip SPA (sinapinic acid) matrix dissolved in an acetonitrile:TFA:water mixture (49.5:0.5:50) was added twice in 1 µl increments and allowed to air-dry. All ProteinChip arrays were analyzed with the ProteinChip SELDI system with an ion acceleration potential of 20 kV and a detector voltage of 2.8 kV. Data processing steps included baseline subtractions and external calibration using a mixture of known peptide and protein calibrants. Peak detection (S/N >3) and peak clustering were performed automatically using ProteinChip data manager software, version 3.2.

Optimization Results

The results of the optimization experiments are shown in Figures 1 and 2.

The data demonstrate that the greatest number of proteins were detected by both 2DGE and SELDI when 100 µl of beads was used with 1,000 µl of sample. Decreasing the amount of

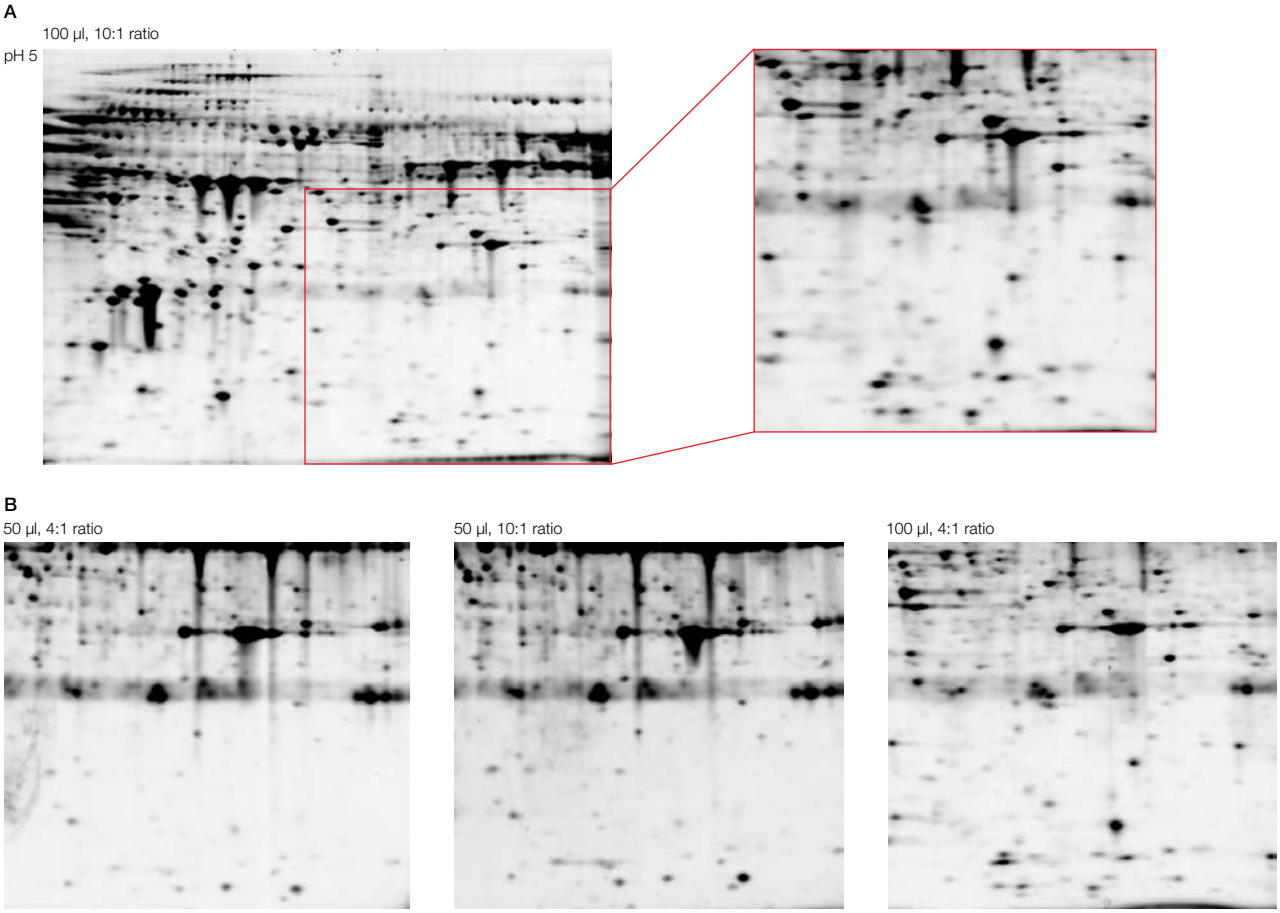

Fig. 1. 2DGE of plasma samples treated with ProteoMiner under optimal conditions with 10:1 or 4:1 sample:bead volume ratios and 50 or 100 µl of beads in a mini spin column. A, 10:1 sample:bead volume and 100 µl of beads using the following 2DGE conditions: 1st dimension, pH 5-8, 11-cm; 2nd dimension, 8-16% Criterion™ precast gels, 100 µg sample, staining with Flamingo™ fluorescent gel stain. Highlighted area used for spot count (Table 1). **B**, Same conditions applied to different sample:bead volume ratios; areas shown correspond to highlighted area from **A**.

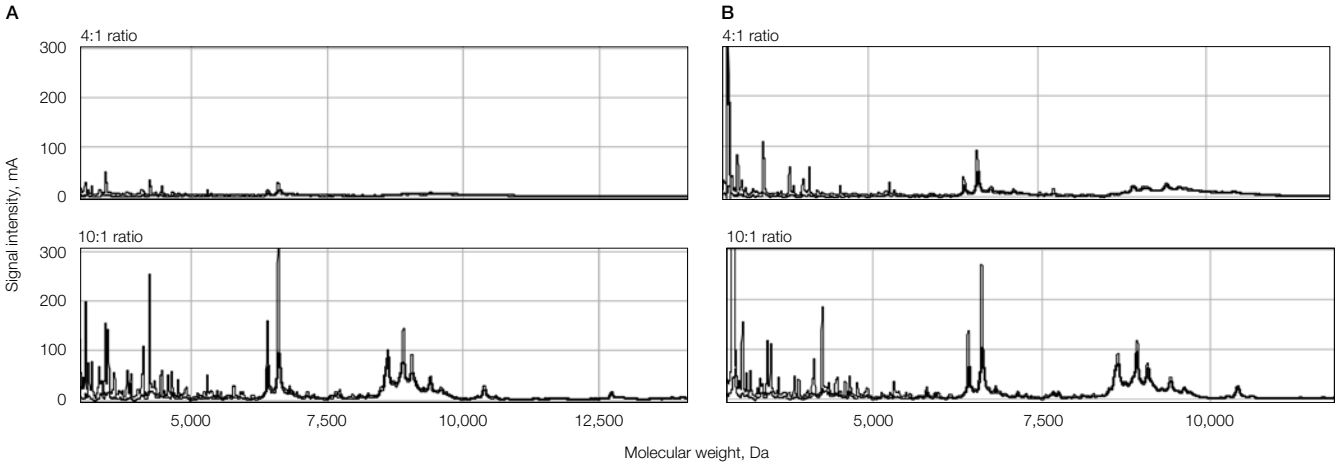

Fig. 2. ProteinChip SELDI system analysis with ProteinChip CM10 array of 4:1 and 10:1 sample-to-bead ratios for both the 50 µl (A) and 100 µl (B) bead volumes. The 10:1 ratios produce the greatest number of peaks.

sample with a constant volume of beads reduced the number of proteins detected. In the highlighted regions from the 2-D gels, 196 spots were detected when 1,000 µl of sample were added to 100 µl of beads, while only 155 spots were detected when the volume was decreased to 400 µl. Similarly, 173 spots were detected when 50 µl of beads were loaded, while only 141 spots were detected when 200 µl were loaded. With both protein volumes (100 and 50 µl), the greatest number of proteins were detected when a 10:1 sample to bead volume ratio was used.

Table 2. Sample and bead volumes tested with resulting peak count data from SELDI runs with ProteinChip CM10 arrays.

Sample Volume, µl	Bead Volume, µl	Sample-to-Bead Ratio	Peak Count
1,000	100	10:1	86
400	100	4:1	81
500	50	10:1	79
200	50	4:1	73

Conclusions

The ProteoMiner protein enrichment system reduces the complexity of samples, in particular serum and plasma samples, by decreasing the amount of high-abundance proteins and enriching low-abundance proteins. This is achieved through a high level of diversity and representation of the hexapeptide library, as well as an appropriate level of saturation of the ligands. Reducing the bead volume decreases the coverage across the proteome, which ultimately reduces the number of proteins that can be captured. Using a smaller sample volume (lower protein load) limits the number of high-abundance proteins that reach saturation, thereby reducing the number of proteins whose concentrations are decreased following treatment. Furthermore, using less sample decreases the total protein loaded onto the beads and therefore lowers the probability of capturing low-abundance proteins. Hexapeptide diversity, saturation level, and protein load all must be optimized to ensure maximum performance of ProteoMiner system technology. For best performance and when possible, we recommend using 1 ml of sample (50 mg/ml) with 100 µl of beads. The 2-D and SELDI data shown here demonstrate that if sample and bead volumes are reduced, fewer spots and peaks are detected, thereby reducing the chance of finding a quantitative difference in a disease versus control sample or, in other words, finding a biomarker candidate.

Reference

Anderson NL and Anderson NG, The human plasma proteome: history, character, and diagnostic prospects, Mol Cell Proteomics 1, 845–867 (2002)

Profinity eXact™ Fusion-Tag System Performs On-Column Cleavage and Yields Pure Native Protein From Lysate in Less Than an Hour

Natalia Oganesyan and William Strong, Bio-Rad Laboratories, Inc. Hercules, CA 94547 USA

Introduction

To simplify purification of recombinant proteins, including many with unknown biochemical properties, several genetically engineered affinity tags, or purification tags, are used. Commonly used tags are polyhistidine (His), glutathione-S-transferase (GST), and the antibody peptide epitope, FLAG (Arnau et al. 2006). The tag is fused to the N- or C-terminus of the protein of interest, allowing the fusion protein to be purified to near homogeneity in a single-step procedure using a resin with strong binding avidity and selectivity to the tag.

Once the fusion protein has been purified, it is often necessary to remove the tag before subsequent use in downstream applications (Arnau et al. 2006, Waugh 2005), because the tag may alter protein conformation (Chant et al. 2005), affect biologically important functions (Araújo et al. 2000, Fonda et al. 2002, Goel et al. 2000), or interfere with protein crystallization (Bucher et al. 2002, Kim et al. 2001, Smyth et al. 2003). The most popular method to remove the tag involves building a protease cleavage site between the tag and the target protein within the expression vector, and cleaving the resultant fusion protein, using purified preparations of the cognate protease specific to the engineered site. The most frequently used processing proteases for this purpose are tobacco etch virus (TEV) protease, thrombin, factor Xa, and enterokinase. Although these tag-removal systems alleviate problems associated with presence of the tag in the final purified protein, they have several principal drawbacks: 1) the high enzyme-to-substrate ratios, the elevated temperatures required for optimal or efficient processing, and the duration of the reaction may affect cleavage specificity as well as stability of the target protein (Arnau et al. 2006, Jenny et al. 2003); 2) the extended length of purification protocols due to additional cleavage and protease-removal steps may hamper high-throughput purification approaches and result in loss of target protein; 3) the nature of protease cleavage mechanisms often result in generation of protein products that still contain extra residues on their N-termini.

These complications can be easily avoided by using the Profinity eXact fusion-tag purification system. The system consists of Profinity eXact purification resin and the Profinity eXact tag, which is a small 8 kD polypeptide expressed as a fusion to the N-terminus of the target protein. The ligand coupled to the resin matrix is based on the bacterial protease subtilisin BPN', which has been extensively engineered to increase stability and to isolate the substrate-binding and proteolytic functions of the enzyme (Abdulaev et al. 2005, Ruan et al. 2004). The incorporated modifications allow for conventional affinity binding with high selectivity, as well as specific and controlled triggering of the highly active cleavage reaction. Cleavage is achieved upon the addition of low concentrations of small anions, such as fluoride or azide. The native recombinant protein is released without any residual amino acids at the N-terminus, and the 8 kD Profinity eXact tag remains bound to the modified subtilisin ligand linked to the resin. Purification of fusion proteins is performed under native conditions, with tag cleavage and elution of purified protein from the column completed in about an hour.

To demonstrate the advantages of the Profinity eXact system one-step protocol, we compared the purification process of maltose-binding protein (MBP) fused either with GST or with the Profinity eXact tag. To mimic the tag-removal capabilities of the Profinity eXact system, the GST-MBP fusions were also engineered with intervening thrombin or TEV cleavage sites. Performance parameters tested in this study include the time required for obtaining tag-free MBP and final yield and purity of the purified protein.

Methods

Vectors and Purification Resins

pGEX2T vector, thrombin protease, and GSTrap HP, HiTrap benzamidine FF, and HisTrap FF columns were purchased from GE Healthcare. AcTEV protease was purchased from Invitrogen Corporation. Profinity eXact pPAL7 expression vector and Bio-Scale™ Mini Profinity eXact™ cartridges (1 ml) were from Bio-Rad Laboratories, Inc.

Expression Vector Construction

The gene encoding MBP was amplified from pMAL vector (Invitrogen) using iProof™ high-fidelity polymerase (Bio-Rad). After digestion with the corresponding restriction enzymes (BamHI and EcoRI), the fragment containing MBP was cloned into pGEX2T vector to obtain a fusion with a thrombin cleavage site (GST-Th-MBP). To obtain the GST-TEV-MBP fusion with AcTEV cleavage site, the sequence encoding the thrombin cleavage site (LVPR^GS) in the vector containing the GST-Th-MBP fusion was replaced by the sequence ENLYFQ^G, using a QuikChange II mutagenesis kit (Stratagene Corporation) according to manufacturer instructions. To obtain Profinity eXact tag-MBP fusion, an MBP-encoded PCR fragment was cloned into the Profinity eXact pPAL7 expression vector using restriction-independent cloning as instructed in the Profinity eXact system manual.

Protein Expression and Purification

The resulting constructs were transformed into *E. coli* BL21(DE3) chemi-competent expression cells (Bio-Rad), and a single clone was grown in autoinduction media overnight at 37°C to allow for induction and expression of the tag-MBP fusion proteins (Studier et al. 2005). Cell lysate was prepared by sonication of the resuspended cell pellet in the purification binding buffer corresponding to each resin matrix: 1x PBS (140 mM NaCl, 2.7 mM KCl, 10 mM Na_2PO_4, 1.8 mM KH_2PO_4) for GSTrap columns, and 0.1 M potassium phosphate buffer, 0.1 mM EDTA, pH 7.2 for Bio-Scale Mini Profinity eXact cartridges. A total of 5 ml of lysate was used for each purification. Fusion protein purification was performed according to manufacturer instructions in a syringe format. Sample and buffer were applied using a syringe attached to the column. In case of GST-MBP fusions, a slow flow rate was maintained during loading and washing (~1 ml/min or 20 drops/min). Elution fractions, 1 ml each, were collected in 1.5 ml tubes. Elution buffer used for the GST gene fusion system (GE Healthcare) was 50 mM Tris-HCl, 10 mM reduced glutathione, pH 8.0. Elution buffer for the Profinity eXact fusion-tag system was 0.1 M potassium phosphate buffer, 0.1 M potassium fluoride, 0.1 mM EDTA, pH 7.2.

Before proceeding to large-scale proteolytic cleavage of the eluted GST-Th-MBP and GST-TEV-MBP fusion proteins, small-scale cleavage reactions were conducted to optimize the enzyme-to-substrate ratio for each of the two proteolytic enymes — thrombin and AcTEV (data not shown). Thrombin cleavage was carried out on-column. The eluate was immediately passed through an inline HiTrap benzamidine FF column to trap the thrombin protease, and the purified MBP was collected in the effluent. Removal of the GST tag from the GST-TEV-MBP fusion was achieved concurrently with buffer exchange by including a His-tagged AcTEV protease during dialysis of the eluted fusion protein in glutathione-free buffer (20 mM Tris-HCl, 0.5 mM EDTA, 5 mM DTT). Tag-free MBP was then obtained in the flow-through fraction after passing the TEV cleavage reaction over a GSTrap column to remove the released GST, immediately followed by a HisTrap column to remove the AcTEV protease.

Preparation of tag-free MBP using the Profinity eXact system was performed according to the standard protocol. The proteolytic activity of the affinity matrix was activated by applying 2 column volumes (CV) of room temperature 0.1 M sodium phosphate buffer, pH 7.2, containing 0.1 M sodium fluoride, to the column and then incubating for 30 min to allow cleavage of the tag from the fusion protein. Purified, tag-free MBP with a native N-terminus was released from the column once flow resumed.

Purity and Yield Determinations

Yield of the tag-free purified MBP was estimated from each purification using A_{280} absorbance and an extinction coefficient of 1.61 mg/ml per one A_{280} unit. Purity was determined by SDS-PAGE analysis using Criterion™ 4–20% Tris-HCl gels (Bio-Rad), followed by staining with Bio-Safe™ Coomassie stain (Bio-Rad) and image acquisition and analysis using a Molecular Imager® GS-800™ calibrated densitometer (Bio-Rad) and Quantity One® 1-D analysis software (Bio-Rad).

Results and Discussion

We purified MBP proteins using the GST gene fusion and Profinity eXact fusion-tag systems, monitoring the duration of the purification, yield, and purity of the tag-free protein. The GE Healthcare protocol for manual purification was chosen as the most comparable method to purify milligram quantities of MBP across the different systems studied.

MBP Purification Using GST-Tag and Enzymatic Tag Removal

We first performed cleavage time-course studies of each enzyme to optimize the digest conditions. A total of 0.1 mg of GST-Th-MBP and GST-TEV-MBP was incubated with 1 U of thrombin or 33, 16, and 8 U of TEV protease. Samples were removed from the digest mixture at various time points and analyzed by SDS-PAGE to estimate the yield, and extent of digestion (for details on experimental conditions, protease amounts, and incubation times, refer to bulletin 5652). Using optimized cleavage conditions, preparative amounts (5 ml of lysate containing approximately 20 mg of fusion protein) of each of the GST-MBP fusions were processed. Fractions from each step in the two protocols were resolved using SDS-PAGE analysis, and results are shown in Figures 1 and 2 for thrombin and TEV cleavage, respectively. In both cases, the final tag-free MBP protein was found to be contaminated with GST.

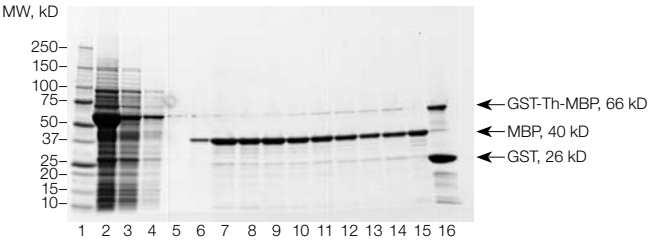

Fig. 1. GST-Th-MBP fusion purification and on-column cleavage with thrombin. Lane 1, Precision Plus Protein™ unstained standards; lane 2, lysate; lane 3, flowthrough; lane 4, wash; lanes 5–14, flow-through fractions from GSTrap and HiTrap benzamidine FF columns containing tag-free MBP; lane 15, pooled fractions (lanes 5–14); lane 16, bound components from GSTrap column.

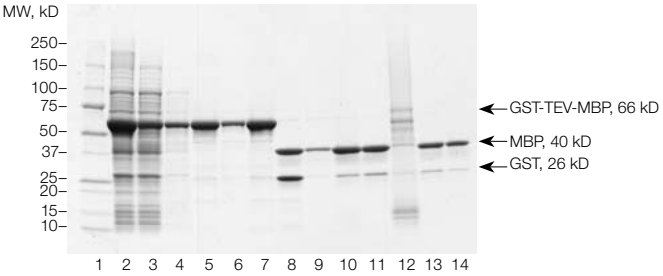

Fig. 2. GST-TEV-MBP fusion purification and cleavage with TEV protease. After cleavage, GST and MBP mixture was passed through a GSTrap column to bind cleaved GST. Collected flowthrough with tag-free MBP was loaded onto a HisTrap FF column to remove His-tagged AcTEV; MBP was collected in the flow-through fraction. Lane 1, Precision Plus Protein unstained standards; lane 2, lysate; lane 3, flowthrough; lane 4, wash; lanes 5–6, fractions containing GST-TEV-MBP fusion protein; lane 7, pooled fractions (lanes 5–6); lane 8, cleaved GST-TEV-MBP fusion; lanes 9–12, purified MBP, flow-through fractions from GSTrap column; lane 13, pooled fractions (lanes 9–12); lane 14, MBP from flowthrough of HisTrap FF column.

Table 1. Summary of MBP purification and cleavage.

Fusion Construct	Cleared Lysate, Starting Material	Purification Steps	Duration of Purification	Yield (Cleaved MBP), mg	Purity, %	Concentration of Final Purified Protein, mg/ml
GST-MBP, thrombin	5 ml, 20 mg fusion protein	5	19 hr	2.0	96.4	0.16
GST-MBP, TEV	5 ml, 20 mg fusion protein	8	20 hr	2.7	96.6	0.39
Profinity eXact MBP	5 ml, 20 mg fusion protein	4	50 min	5.0	98.0	0.90

MBP Purification Using the Profinity eXact Fusion-Tag System

Purification of MBP using the Profinity eXact system was a one-step process. After loading 5 ml of the lysate (~20 mg of fusion protein) onto the Profinity eXact 1 ml column, the column was washed with 1 ml of 1 M sodium acetate in binding buffer (0.1 M potassium phosphate buffer, pH 7.2, 0.1 mM EDTA) and then with 15 ml of binding buffer. Washed resin was saturated with 1 ml of the cleavage buffer (binding buffer containing 0.1 M sodium fluoride) and the column was incubated for 30 min at room temperature. Tag-free MBP was eluted by applying 5 ml of cleavage buffer in 1 ml aliquots (Figure 3). The column was regenerated by stripping the tightly bound Profinity eXact tag (Kd <100 pM) from the resin, by decreasing the pH to below 2.0 using 3 CV of 0.1 M phosphoric acid.

Table 1 summarizes data for the purification experiments. In all the parameters used to gauge the success of purification, the Profinity eXact system performed better than the GST system coupled to either thrombin or TEV cleavage. The use of the Profinity eXact tag and purification resin resulted in nearly 2-fold higher MBP protein yields, when starting from a fixed amount of fusion protein and carrying it through the process to a tag-free form. The lower yields with protocols using GST tags are presumably due to the additional purification steps and possible system sensitivities to the flow rate, which were hard to control in the syringe format. Purity of MBP proteins using the Profinity eXact system was higher than the GST-based purifications, with no visible contaminants in SDS-PAGE analysis using a 3 µg sample load. The product was not appreciably contaminated with the affinity tag or bacterial proteins even at a 10 µg load, as illustrated in Figure 4.

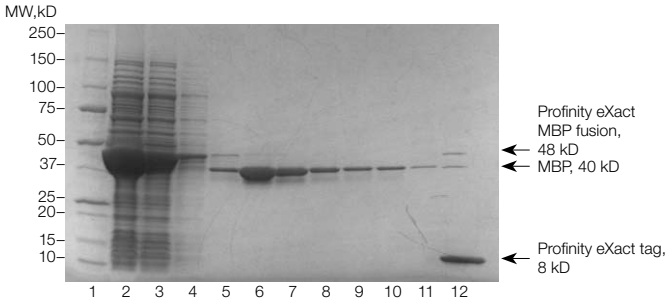

Fig. 3. MBP purification using Profinity eXact tag. Lane 1, Precision Plus Protein unstained standards; lane 2, lysate; lane 3, flowthrough; lane 4, wash; lanes 5–11, tag-free MBP in elution fractions; lane 12, Profinity eXact tag (~8 kD), stripped from the column using 0.1 M phosphoric acid.

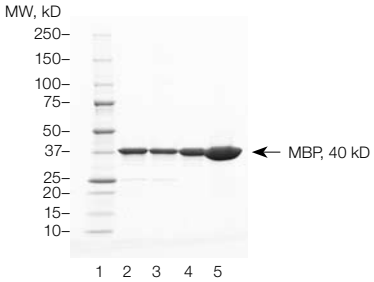

Fig. 4. Purity analysis of isolated MBP using GST fusion and enzymatic tag removal or eXact tag fusion and one-step on-column tag removal. Lane 1, Precision Plus Protein unstained standards; lanes 2–5, MBP protein purified using different methods; lane 2, purified as GST-fusion, tag cleaved with thrombin; lane 3, purified as GST-fusion, tag cleaved with AcTEV; lane 4–5, purified as eXact-tag fusion; lanes 2–4 contained 3 µg sample protein per lane; lane 5 contained 10 µg sample protein per lane.

Conclusions

With the Profinity eXact fusion-tag system, fewer steps are required to reach the tag-free form of the target protein, and the duration of the purification process is considerably reduced from nearly a day to less than 1 hr. The use of the Profinity eXact system also results in the eluted tag-free protein in a more concentrated form. Unlike the thrombin and TEV cleavage systems that leave terminal GS and G residues, respectively, MBP purified with the Profinity eXact system is in its native form and is amenable to direct use in downstream applications.

References

Abdulaev NG et al., Bacterial expression and one-step purification of an isotope-labeled heterotrimeric G-protein α-subunit, J Biomol NMR 32, 31–40 (2005)

Araújo A et al., Influence of the histidine tail on the structure and activity of recombinant chlorocatechol 1,2-dioxygenase, Biochem Biophys Res Commun 272, 480–484 (2000)

Arnau J et al., Current strategies for the use of affinity tags and tag removal for the purification of recombinant proteins, Protein Expr Purif 48, 1–13 (2006)

Bucher MH et al., Differential effects of short affinity tags on the crystallization of *Pyrococcus furiosus* maltodextrin-binding protein, Acta Crystallogr D Biol Crystallogr 58, 392–397 (2002)

Chant A et al., Attachment of a histidine tag to the minimal zinc finger protein of the *Aspergillus nidulans* gene regulatory protein AreA causes a conformational change at the DNA-binding site, Protein Expr Purif 39, 152–159 (2005)

Fonda I et al., Attachment of histidine tags to recombinant tumor necrosis factor-alpha drastically changes its properties, ScientificWorldJournal 2, 1312–1325 (2002)

Goel A et al., Relative position of the hexahistidine tag effects binding properties of a tumor-associated single-chain Fv construct, Biochim Biophys Acta 1523, 13–20 (2000)

Jenny RJ et al., A critical review of the methods for cleavage of fusion proteins with thrombin and factor Xa, Protein Expr Purif 31, 1–11 (2003)

Kim KM et al., Post-translational modification of the N-terminal His tag interferes with the crystallization of the wild-type and mutant SH3 domains from chicken src tyrosine kinase, Acta Crystallogr D Biol Crystallogr 57, 759–762 (2001)

Ruan B et al., Engineering subtilisin into a fluoride-triggered processing protease useful for one-step protein purification, Biochemistry 43, 14539–14546 (2004)

Smyth DR et al., Crystal structures of fusion proteins with large-affinity tags, Protein Sci 12, 1313–1322 (2003)

Studier FW, Protein production by auto-induction in high-density shaking cultures, Protein Expr Purif 41, 207–234 (2005)

Waugh DS, Making the most of affinity tags, Trends Biotechnol 23, 316–320 (2005)

For an expanded version of this article, request bulletin 5652.

MYCN
TP53

Real-Time qPCR as a Tool

for Evaluating RNAi-Mediated Gene Silencing

Real-time quantitative PCR (rt-qPCR) is the method of choice for accurate, sensitive, and specific quantitation of nucleic acid sequences. Applications of this technology are numerous, both in molecular diagnostics and in virtually all fields of life sciences, including gene expression profiling, measurement of DNA copy number alterations, genotyping, mutation detection, pathogen detection, measurement of viral load, disease monitoring, and assessment of drug response. Several ingredients are essential to the successful and reliable completion of an rt-qPCR assay, such as careful primer design and evaluation, template preparation, the use of a robust normalization strategy, and accurate data analysis. This article describes how rt-qPCR can be implemented as a tool to monitor silencing efficiency and functional effects of RNA interference (RNAi)-mediated gene knockdown, using examples from our research on neuroblastoma. For detailed information on the experiments that contributed to this research, including instruments, reagents, and procedures, request bulletin 5692.

Authors: Tom Van Maerken, Pieter Mestdagh, Sarah De Clercq, Filip Pattyn, Nurten Yigit, Anne De Paepe, Jean-Christophe Marine, Frank Speleman, and Jo Vandesompele

Neuroblastoma and the *MYCN* and *TP53* Cancer Genes

Neuroblastoma is a childhood cancer derived from precursor cells of the adrenosympathetic system, arising in the adrenal medulla or in sympathetic ganglia. Although a relatively rare form of cancer, neuroblastoma is among the most fatal of childhood diseases. Indicators of mortality include age at diagnosis (the outcome for children with neuroblastoma is most favorable when diagnosed before the age of one year, even when the disease has metastasized), tumor stage, and level of MYCN protein activity (the most fatal clinicogenetic subtype of neuroblastoma is characterized by amplification of the *MYCN* oncogenic transcription factor) (Vandesompele et al. 2005). The mechanisms by which this transcription factor exerts its oncogenic activity and confers an unfavorable prognosis are poorly understood.

Another intriguing feature of neuroblastoma is the remarkably low frequency of *TP53* mutations at diagnosis (Tweddle et al. 2003). Previous studies have shown that reactivation of the p53 pathway by the selective small-molecule MDM2 antagonist nutlin-3 constitutes a promising novel therapeutic approach for neuroblastoma (Van Maerken et al. 2006). To gain insight into the mechanism of action of these two pivotal genes in neuroblastoma pathogenesis and to create model systems for future exploration of targeted therapeutics in relationship to *MYCN* and *TP53* status, RNAi was used as an experimental tool for suppressing the expression of these genes. Because neuroblastomas are notoriously difficult to transfect, we introduced an siRNA model with accurate detection of silencing efficiency and the resulting effects. In particular, for study of *MYCN* function, this model is believed to be more relevant, because traditional systems with forced overexpression of this gene in single-copy cells seem to lack the proper cellular context to mimic endogeneous amplification and hyperactivity. Our final goal is to disentangle *MYCN*'s transcriptional web, in order to interfere with its oncogenic signaling pathways, while leaving the beneficial pathways unaltered.

From Experimental Design to Analysis of an rt-qPCR Assay

Purity and integrity of the template are critical factors to the success of an rt-qPCR assay. Several commercial kits are available for producing clean RNA samples. Contaminants should be avoided or removed, as they can greatly influence the reverse-transcription step or the actual PCR. The presence of PCR inhibitors can be determined by a variety of methods, including the simple and fast PCR-based SPUD assay (Nolan et al. 2006). An oligonucleotide target sequence with no homology to human DNA is spiked into human RNA samples and a water control at a known concentration. rt-qPCR quantitation of the oligonucleotide template in both the RNA samples and the (negative) water control is indicative of possible enzymatic inhibitors present in the RNA extract. For assessment of RNA integrity, electrophoresis and PCR-based methods are available (Fleige and Pfaffl 2006, Nolan et al. 2006). Figure 1 shows an electropherogram of high-quality RNA assessed using the Experion™ automated electrophoresis system. Sharp peaks at 18S and 28S and no nonspecific peaks are desired results when determining whether or not RNA samples are intact.

The Many Faces of Disease

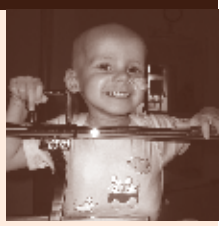

With the focus of his research in neuroblastoma, a very deadly form of childhood cancer, Professor Jo Vandesompele often gets asked if he meets the children behind the research. His answer: "No, we see a tube." In fact, most researchers spend countless hours with analytical tools, but little time, if any, interacting with people affected by disease. That's why the scientists that comprise Vandesompele's lab at Ghent University in Belgium are introducing a pilot program, where parents of children who have died or are suffering from neuroblastoma will be invited to speak to researchers about their experiences.

"Most of us don't maintain a sense of what we're doing research for," says Vandesompele. "A sample is brought from a hospital lab. We begin extracting molecules and conducting procedures that have nothing to do with the child the sample came from, a child who might be dying. There's a disconnect there that shouldn't be." The parent program is meant to bridge this disconnect.

The idea sprang from travels to international conferences, where parents involved in disease-related support groups occasionally give talks. Vandesompele's colleagues realized that in terms of motivating progress toward a cure, even the world's best scientists can't match the words of a parent whose child has died. And it's not just that parents have heartbreaking tales to tell. It's also that they have a passion for raising money to support research, and that they're truly interested in what's happening in the field.

"Yes, we're doing science," says Vandesompele, "but being connected to the human aspects of research can motivate scientists to be much more precise, closer to perfect in what we are doing. Passion brings us to a level unattainable based on intellectual skills alone."

Soon, at least in Belgium, researchers will begin to be able to match a name and a face to a test tube.

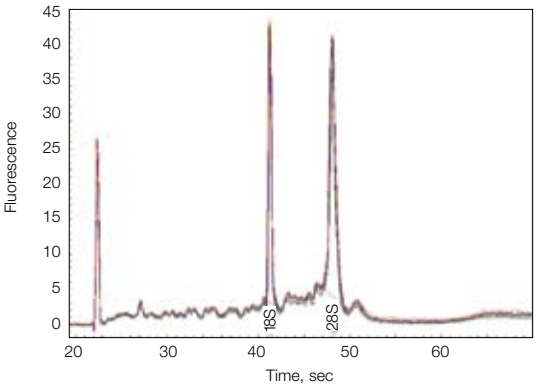

Fig. 1. Electropherogram generated using the Experion system depicting high-quality RNA sample.

To control for inevitable experimental variation due to factors such as the amount and quality of starting material, enzymatic efficiencies, and overall cellular transcriptional activity, use of a reliable normalization strategy in which these factors are taken into account is necessary. In principle, internal reference genes offer the best way to deal with the multiple sources of variables that might exist between different samples. A truly accurate normalization can only be achieved when multiple reference genes are utilized, as use of a single reference gene results in relatively large errors in a considerable proportion of the sample set (Vandesompele et al. 2002). Care should be taken when selecting the genes to be used for normalizing the expression levels since no universal set of always-applicable reference genes exists. Different sample origins and experimental manipulations might require another set of genes to be used as reference genes. The selection and validation of reference genes can be done using the geNorm algorithm (see sidebar), which determines the most stable genes from a set of tested candidate reference genes in a given sample panel and calculates a normalization factor (Vandesompele et al. 2002).

Bioinformatics-based quality assessment of newly designed rt-qPCR primers can considerably improve the likelihood of obtaining specific and efficient primers. A number of quality control parameters have been integrated in Ghent University's RTPrimerDB in silico assay evaluation pipeline (Pattyn et al. 2006). This pipeline allows a streamlined evaluation of candidate primer pairs, with automated BLAST specificity search, prediction of putative secondary structures of the amplicon, indication of which transcript variants of the gene of interest will be amplified, and search for known SNPs in the primer annealing regions. This in silico evaluation, however, does not preclude the need for experimental validation after synthesis of the primers. Ideally, experimental evaluation addresses specificity, efficiency, and dynamic range of the assay using a broad dilution series of template (Figure 2).

Processing and analysis of the raw rt-qPCR data represent a multistep computational process of averaging replicate C_T values, normalization, and proper error propagation along the entire calculation track. This process might prove cumbersome and deserves equal attention as the previous steps in order to get accurate and reliable results. This final procedure has been automated and streamlined in Biogazelle's qBasePlus software (www.biogazelle.com, see sidebar), a dedicated program for the management and analysis of rt-qPCR data (Hellemans et al. 2007).

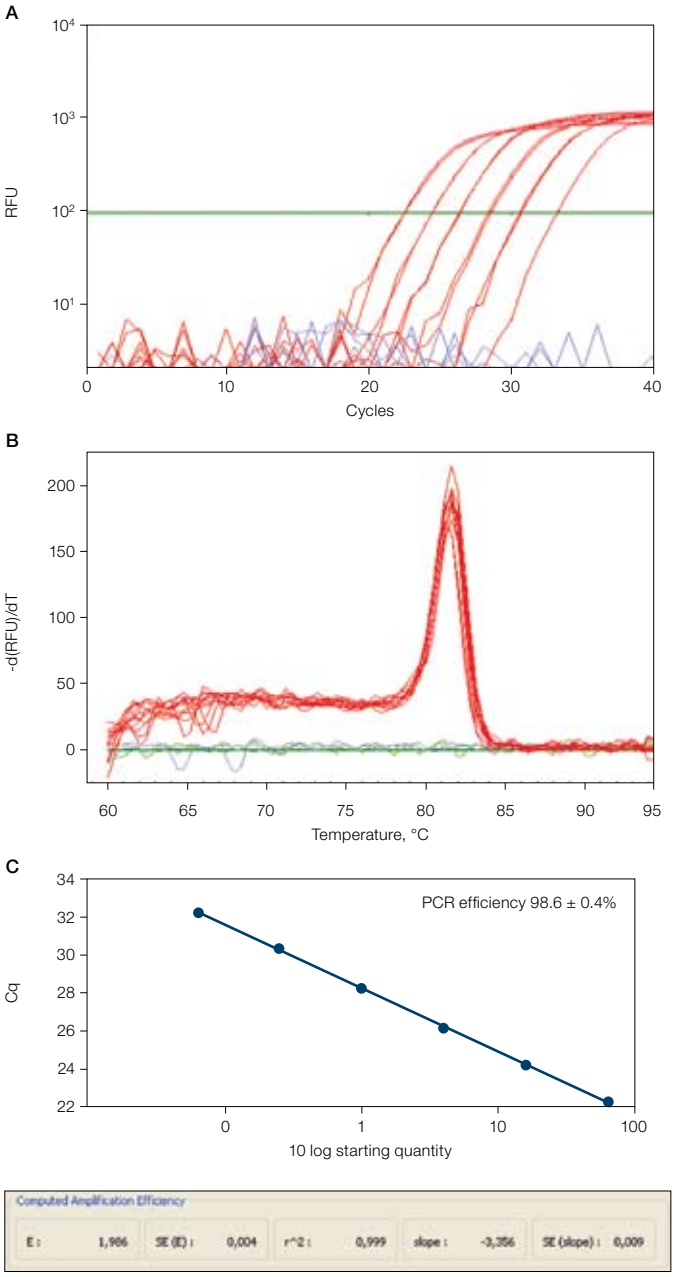

Fig. 2. Experimental validation of newly designed rt-qPCR primers. A, PCR efficiency and dynamic range of the rt-qPCR assay was tested using a 4-fold serial dilution of six points of reverse transcribed human qPCR reference total RNA (64 ng down to 62.5 pg) and TP53_P2 primers; **B**, specificity of the TP53_P2 primers was assessed by generating a melting curve of the PCR product; **C**, standard curve and PCR efficiency estimation (including the error) according to the qBase*Plus* software. C_q, quantitation cycle value generated in RDML software (see sidebar).

rt-qPCR for Assessment of siRNA Silencing Efficiency: Anti-*MYCN* siLentMer™ siRNA Duplexes

Human IMR-32 neuroblastoma cells were transfected with different anti-*MYCN* siLentMer siRNA duplexes or a nonspecific control siRNA, and the *MYCN* transcript level was determined 48 hours posttransfection by rt-qPCR. Our results indicate the importance of primer location for evaluation of siRNA silencing efficiency, in agreement with a previous independent report (Shepard et al. 2005). The target mRNA sequence is cleaved by the RNA-induced silencing complex (RISC) near the center of the region complementary to the guiding siRNA (Elbashir et al. 2001). Complete nucleolytic degradation of the resulting fragments is not always guaranteed, which might result in underestimation of siRNA silencing efficiency if primers are used that do not span the siRNA target sequence, as observed for this gene (Figure 3).

Programming Progress

The year 2000 is a milestone that symbolizes movement toward the height of progress, particularly in science and technology. But back in 2000, Professor Jo Vandesompele (then a doctorate student beginning what would become a career devoted to the study of the genetics of neuroblastoma at Ghent University in Belgium) was attempting to conduct sophisticated analysis of genetic research results with rudimentary tools. "In 2000," says Vandesompele, "evaluating candidate reference genes with respect to their expression stability was impossible." Moreover, the concept of accurate normalization using multiple reference genes did not exist. "The problem of housekeeping gene variability was significantly underestimated at that time," he explains. In addition, he remembers calculating qPCR analyses by hand with Excel software, "a slow and error-prone process that required insight into mathematics and various quantitation models."

With no other solutions available, Vandesompele and colleagues set out to develop the first of many software, web, and database tools that continue to help drive progress in genetic research — not just in their lab, but in labs across the world. Launched in 2002, geNorm software is a tool used for the identification of stably expressed reference genes (**http://medgen.ugent.be/genorm/**). This launch was quickly followed by development of RTPrimerDB in 2003, a real-time PCR primer and probe database containing published and validated assays, as well as an integrated in silico PCR assay evaluation pipeline (**http://medgen.ugent.be/rtprimerdb/**).

In 2004, Jan Hellemans, a PhD student in the University's Center for Medical Genetics laboratory, began automating the arduous mathematical computations associated with qPCR analysis by programming a few simple macros in Excel. These initial macros evolved into the qBase 1.0 qPCR data analysis software package (**http://medgen.ugent.be/qbase/**). Since then, several thousand copies have been downloaded and used worldwide. In 2007, the Excel version began being phased out by qBase*Plus*, a professional Java-based application that runs 20 times faster and is more intuitive than the original platform. All current versions of these programs are available at no charge, and even this latest tool developed by Biogazelle, a Ghent University spin-off company, will offer both free and reasonably priced licensing packages.

That these programs have revolutionized the synthesis of real-time PCR data is unquestionable. What is surprising, at least to Vandesompele, is that "what were once just tools to measure gene expression levels in scarce tumor biopsies from children with neuroblastoma in our laboratory, have now grown in scope to form an independent research line."

And while researchers in this lab continue to try to find new ways to combat neuroblastoma, so will they continue to discover tools to aid achievement of reliable and meaningful results through bioinformatics. Future plans include establishment of an international consortium to finalize a standard exchange format for real-time PCR data (coined RDML, previews of this effort can be seen at **www.rdml.org**). In addition, they are developing a web-based primer design portal that will enable researchers to design high-quality assays in a high-throughput environment.

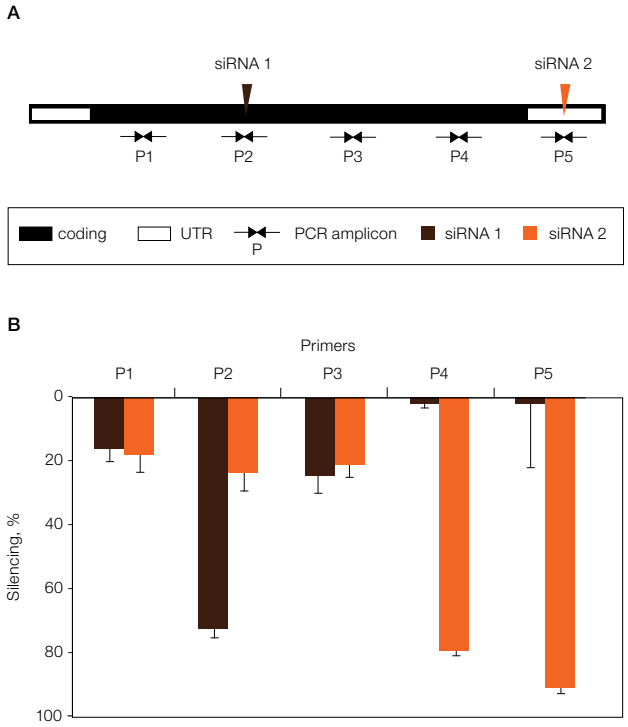

Fig. 3. Importance of primer location for rt-qPCR assessment of siRNA silencing efficiency. A, schematic representation of the *MYCN* mRNA structure with location of siRNA targeted sequences and primer binding sites; **B**, percentage silencing of *MYCN* gene expression measured by five different primer pairs (P1–P5) in IMR-32 cells 48 hr posttransfection with anti-*MYCN* siLentMer siRNA duplexes (siRNA 1 or siRNA 2), compared to cells transfected with a nonspecific control siRNA.

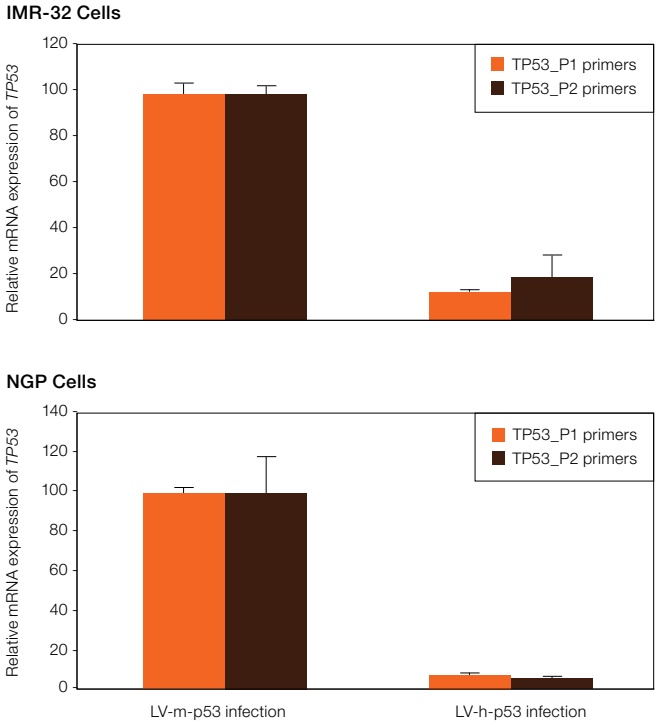

Fig. 4. Assessment of shRNA-mediated *TP53* knockdown efficiency by rt-qPCR. IMR-32 and NGP cells were infected with a lentivirus carrying an shRNA construct specific for either the human *TP53* gene (LV-h-p53) or the murine *Trp53* gene (LV-m-p53) as a control. Efficiency of *TP53* gene silencing was evaluated by rt-qPCR using two different primer pairs (TP53_P1 and TP53_P2). Bars indicate mRNA expression levels of *TP53* relative to the respective LV-m-p53 cells; error bars depict standard error of the mean (duplicated PCR reactions for *TP53* and three reference genes).

rt-qPCR for Monitoring of shRNA Silencing Efficiency and Functional Effects: Lentiviral-Mediated shRNA Knockdown of *TP53*

For generation of stable *TP53* knockdown variants of neuroblastoma cell lines with wild-type p53, we infected IMR-32 and NGP cells with a lentiviral vector encoding an shRNA directed specifically against human *TP53* (LV-h-p53) or against the murine *Trp53* gene (LV-m-p53, negative control). rt-qPCR analysis with two different primer pairs demonstrated that expression of *TP53* was reduced by 81–87% in IMR-32-LV-h-p53 cells and by 92–94% in NGP-LV-h-p53 cells compared to the respective LV-m-p53 controls (Figure 4). Functionality of the *TP53* knockdown variants was validated by rt-qPCR and cell viability analysis after treatment of the cells with nutlin-3, a small-molecule compound that selectively disrupts the interaction between p53 and its negative regulator *MDM2*, resulting in stabilization and

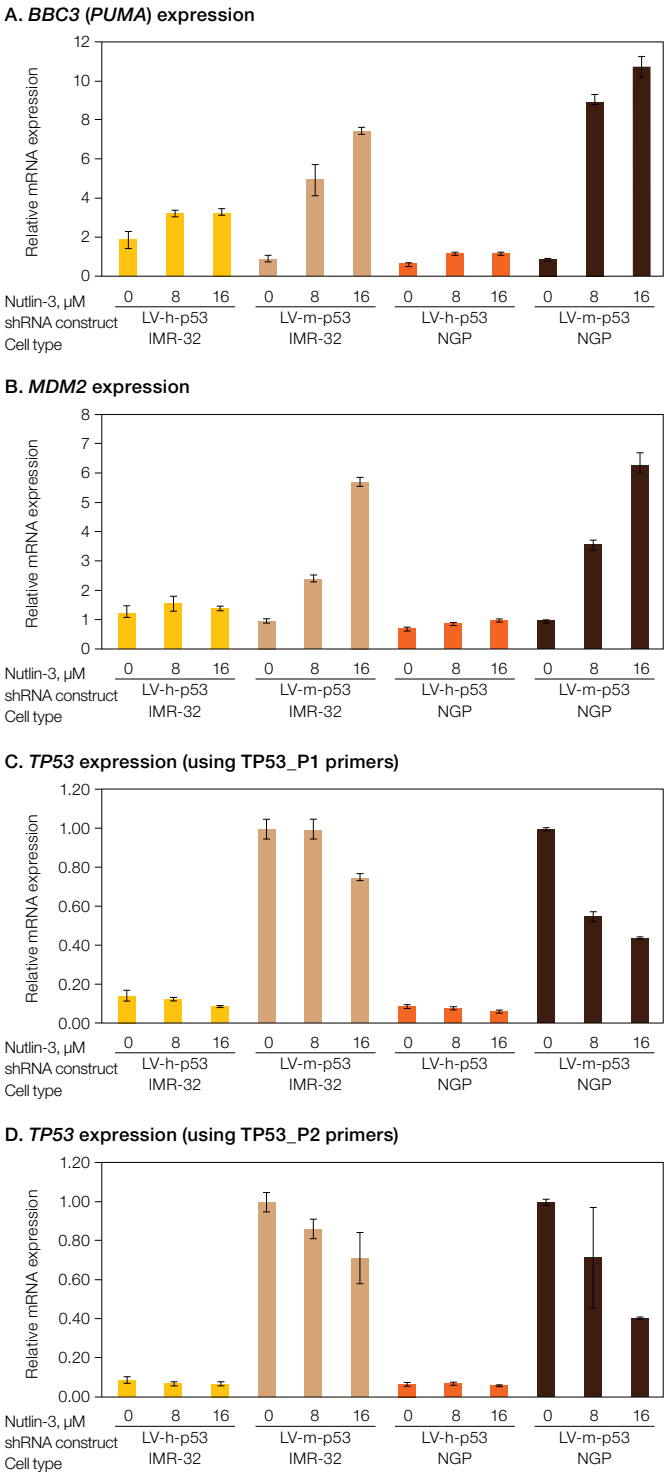

Fig. 5. Functional validation of shRNA-mediated *TP53* knockdown through rt-qPCR analysis of transcript levels of p53-regulated genes after nutlin-3 treatment. IMR-32 and NGP cells were infected with a lentiviral vector encoding an shRNA directed specifically against either the human *TP53* gene (LV-h-p53) or the murine *Trp53* gene (LV-m-p53). Cells were treated with 0, 8, or 16 µM nutlin-3 for 24 hr, and expression of *BBC3* (*PUMA*) (**A**), and *MDM2* (**B**), p53-regulated genes, and *TP53* was determined by rt-qPCR. Two different primer pairs (TP53_P1 and TP53_P2) were used for quantitation of *TP53* transcript levels (**C**,**D**). Bars indicate mRNA expression levels relative to the respective vehicle-treated (0 µM nutlin-3) LV-m-p53 infected cells, mean of two different rt-qPCR measurements; error bars show standard error of the mean.

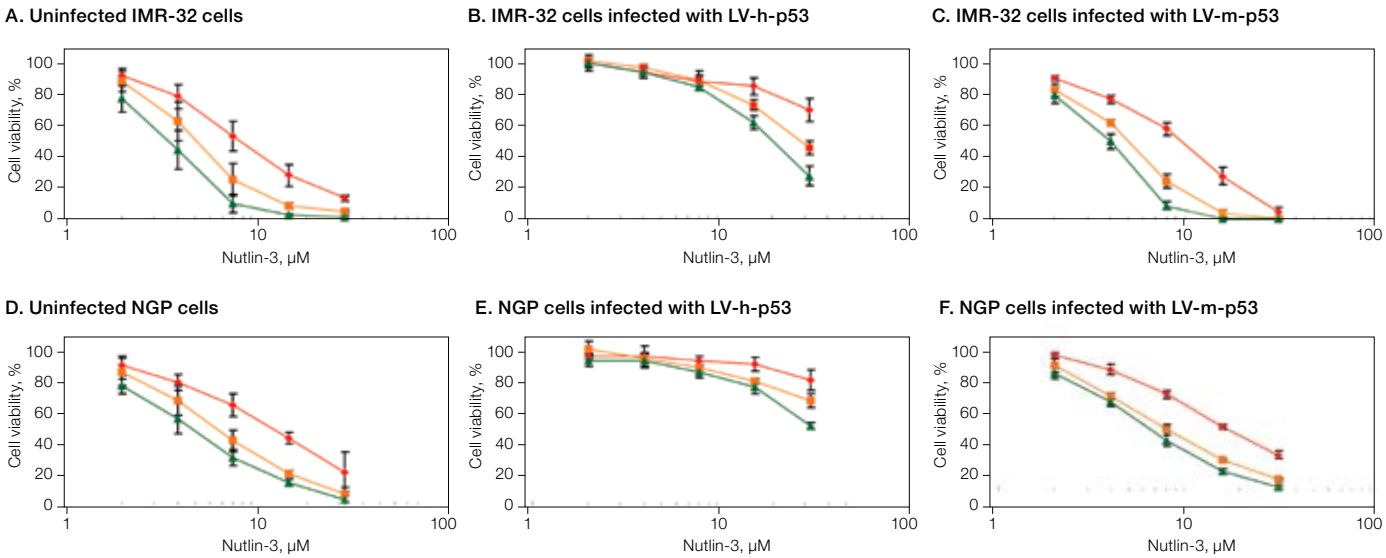

Fig. 6. Functional validation of shRNA-mediated *TP53* knockdown through cell viability analysis after treatment of IMR-32 and NGP cells with nutlin-3. Effect of nutlin-3 on viability of uninfected cells (**A**, **D**), LV-h-p53 infected cells (**B**, **E**) and LV-m-p53 infected cells (**C**, **F**). Exponentially growing cells were exposed to 0–32 µM of nutlin-3 for 24 (—), 48 (—), and 72 (—) hr, and the percentage cell viability with respect to vehicle-treated cells was determined. Error bars indicate standard deviation of mean cell viability values of three independent experiments.

accumulation of the p53 protein and activation of the p53 pathway (Vassilev et al. 2004). Transactivation of p53 target genes such as *BBC3* (*PUMA*) and *MDM2* by nutlin-3 and nutlin-3 induced downregulation of *TP53* mRNA level, a consequence of the ability of the p53 protein to negatively regulate its own transcriptional expression after accumulation (Hudson et al. 1995), were largely prevented by lentiviral-mediated expression of shRNA against human *TP53* (Figure 5). At the cellular level, silencing of human *TP53* severely attenuated the nutlin-3 induced reduction in cell viability observed in nontransduced parental cells, in contrast to control infection with LV-m-p53 (Figure 6). These results firmly demonstrate potent and selective impairment of p53 function in IMR-32-LV-h-p53 and NGP-LV-h-p53 cells.

Conclusions

rt-qPCR analysis provides a convenient and reliable method for evaluation of knockdown efficiency and functional consequences of RNAi-mediated gene silencing. Successful application of this monitoring tool requires careful attention to be given to all different steps in the rt-qPCR workflow, including primer design and evaluation, template preparation, normalization strategy, and data analysis, as discussed in this article.

Similar studies will be conducted in the future to evaluate results achieved using additional cell lines and varying combinations of multiple siLentMer duplexes, durations of effect, and concentrations of active siLentMer duplexes.

References

Elbashir SM et al., RNA interference is mediated by 21- and 22-nucleotide RNAs, Genes Dev 15, 188–200 (2001)

Fleige S and Pfaffl MW, RNA integrity and the effect on the real-time qRT-PCR performance, Mol Aspects Med 27, 126–139 (2006)

Hellemans J et al., qBase relative quantification framework and software for management and automated analysis of real-time quantitative PCR data, Genome Biol 8, R19 (2007)

Hudson JM et al., Wild-type p53 regulates its own transcription in a cell-type specific manner, DNA Cell Biol 14, 759–766 (1995)

Nolan T et al., Quantification of mRNA using real-time RT-PCR, Nat Protoc 1, 1559–1582 (2006)

Nolan T et al., SPUD: a quantitative PCR assay for the detection of inhibitors in nucleic acid preparations, Anal Biochem 351, 308–310 (2006)

Pattyn F et al., RTPrimerDB: the real-time PCR primer and probe database, major update 2006, Nucleic Acids Res 34, D684–D688 (2006)

Shepard AR et al., Importance of quantitative PCR primer location for short interfering RNA efficacy determination, Anal Biochem 344, 287–288 (2005)

Tweddle DA et al., The p53 pathway and its inactivation in neuroblastoma, Cancer Lett 197, 93–98 (2003)

Vandesompele J et al., Unequivocal delineation of clinicogenetic subgroups and development of a new model for improved outcome prediction in neuroblastoma, J Clin Oncol 23, 2280–2299 (2005)

Vandesompele J et al., Accurate normalization of real-time quantitative RT-PCR data by geometric averaging of multiple internal control genes, Genome Biol 3, RESEARCH0034 (2002)

Van Maerken T et al., Small-molecule MDM2 antagonists as a new therapy concept for neuroblastoma, Cancer Res 66, 9646–9655 (2006)

Vassilev LT et al., In vivo activation of the p53 pathway by small-molecule antagonists of MDM2, Science 303, 844–848 (2004)

Grant support: the Fund for Scientific Research – Flanders (FWO) grants 011F4004 (T. Van Maerken, Research Assistant), G.1.5.243.05 (J. Vandesompele) and G.0185.04; GOA grant 12051203; grants from the Belgian Foundation against Cancer (S. De Clercq), the Ghent Childhood Cancer Fund, and the Ghent University Research grant (B.O.F.) 01D31406 (P. Mestdagh).

Contact information: Jo Vandesompele, Center for Medical Genetics, Ghent University Hospital, MRB, De Pintelaan 185, 9000 Ghent, Belgium. Phone: 32-9-332-5187; Fax: 32-9-332-6549; E-mail: Joke.Vandesompele@UGent.be

Simple and Rapid Optimization of Transfections Using Preset Protocols on the Gene Pulser MXcell™ Electroporation System

Joseph Terefe, Maxinne Pineda, Elizabeth Jordan, Luis Ugozzoli, Teresa Rubio, and Michelle Collins, Bio-Rad Laboratories, Inc., Hercules, CA 94547 USA

Introduction

The ability to modulate gene expression is essential to achieving a better understanding of gene function. The transfer of exogenous nucleic acids, such as plasmids or siRNAs, into mammalian cells is an important tool for the study and analysis of gene function, expression, regulation, and mutation, and has advanced basic cellular research, drug target identification, and validation. Electroporation is a well-established gene transfer method and an effective means of transferring nucleic acids into cells. Finding optimal transfection conditions is crucial in a gene transfer experiment to obtain the highest transfection efficiency with maximum cell viability. There are many parameters that affect the efficiency of electroporation, including waveform (exponential or square-wave), voltage, capacitance, resistance, pulse duration, and number of pulses.

The Gene Pulser MXcell electroporation system and Gene Pulser® electroporation buffer were designed to address the need for attaining the highest transfection efficiency and cell viability in mammalian cells. The Gene Pulser MXcell system is an open platform that provides the flexibility for creating specific protocols and varying parameters, including the unique option of providing both square and exponential waveforms in the same instrument. Preset and gradient protocols allow easy optimization of all parameters. Preset protocols are defined for whole or partial (mini protocol) plates, depending on cell availability. A preset protocol decision tree is shown in Figure 1.

Here, we demonstrate using Gene Pulser electroporation buffer with preset protocols to achieve maximum transfection efficiency and cell viability.

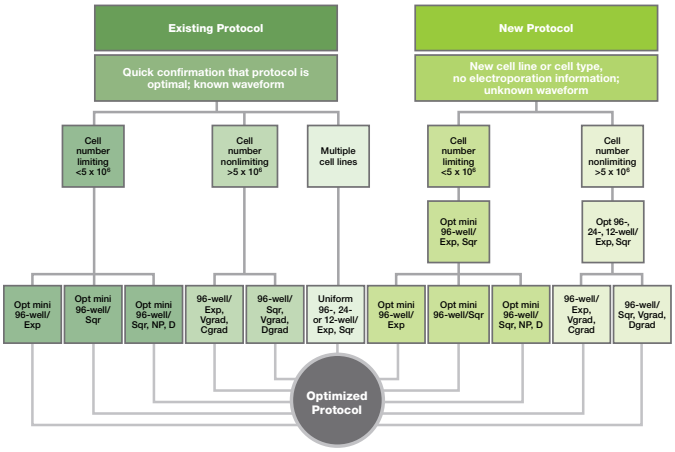

Fig. 1. Gene Pulser MXcell system preset protocol decision tree.

Methods

Cell Lines, Plasmids, and siRNAs

Cells were obtained from American Type Culture Collection (ATCC). HeLa cells (#CCL-2) were cultured in Dulbecco's modified Eagle's medium containing 1 mM sodium pyruvate, 0.1 mM nonessential amino acids, and 10% fetal bovine serum (FBS). CHO-K1 cells (#CCL-61) were cultured in Ham's F-12K medium supplemented with 10% FBS.

For optimization of siRNA delivery, fluorescently labeled siLentMer™ Dicer-substrate siRNA duplexes, targeting the glyceraldehyde-3-phosphate dehydrogenase gene (GAPDH) or negative controls, were used. Negative control and luciferase-specific siRNAs were also used. For the optimization of plasmid delivery, a plasmid DNA expressing the luciferase gene (pCMVi-Luc) was used.

Electroporation

Cells were used at a density of 1 x 10^6 cells/ml, unless indicated otherwise. Electroporation was performed in either 96- or 24-well electroporation plates. After harvesting by trypsinization, cells were washed with phosphate buffered saline (PBS), counted, and the appropriate number of cells per experiment was aliquoted. Before electroporation, cells were resuspended in Gene Pulser electroporation buffer, and plasmid DNA (10 µg/ml) or siLentMer siRNA (100 nM) was added to the mix. Then, the cells were transferred to electroporation plates (96- or 24-well) and pulsed with the Gene Pulser MXcell electroporation system. Electroporated cells were transferred to tissue culture plates containing the appropriate growth medium and incubated at 37°C for 24 hr. Prior to harvesting, cell viability was assessed by visual inspection and by comparing cell confluency between different conditions.

Analysis of Transfection

Cells electroporated with the pCMVi-Luc plasmid were assayed for luciferase activity. Cells electroporated with fluorescently labeled siRNA were washed with PBS, trypsinized, pelleted, and resuspended in PBS for analysis by flow cytometry or fluorescence microscopy. Delivery of the GAPDH siLentMer siRNA was also assessed by real-time quantitative (rt-qPCR). Total RNA was extracted from electroporated cells (Aurum™ total RNA kit) and used for cDNA synthesis (iScript™ cDNA synthesis kit), followed by rt-PCR using gene-specific primers and iQ™ SYBR® Green supermix on the iQ™5 real-time PCR detection system (all from Bio-Rad) to analyze for gene silencing.

Results and Discussion

siRNA Delivery Into HeLa Cells

To define the best conditions for siRNA delivery, HeLa cells were electroporated on the Gene Pulser MXcell system with a negative control or GAPDH-specific siLentMer siRNA using the preset protocol Opt mini 96-well/Exp, Sqr in a 96-well format. This protocol uses three square-wave and three exponential decay conditions in six well sets as shown in Figure 2A. Gene silencing was used as a measure of the transfection efficiency for siRNA delivery (Figure 2B, C). Using this protocol, conditions in well set 2 (250 V, 2,000 µF, 20 ms) were found to be optimal. Cell viability was high as measured by cell confluency, and a greater than 95% reduction in transcript levels was observed in cells electroporated with siRNA targeting GAPDH compared to those electroporated with the negative control.

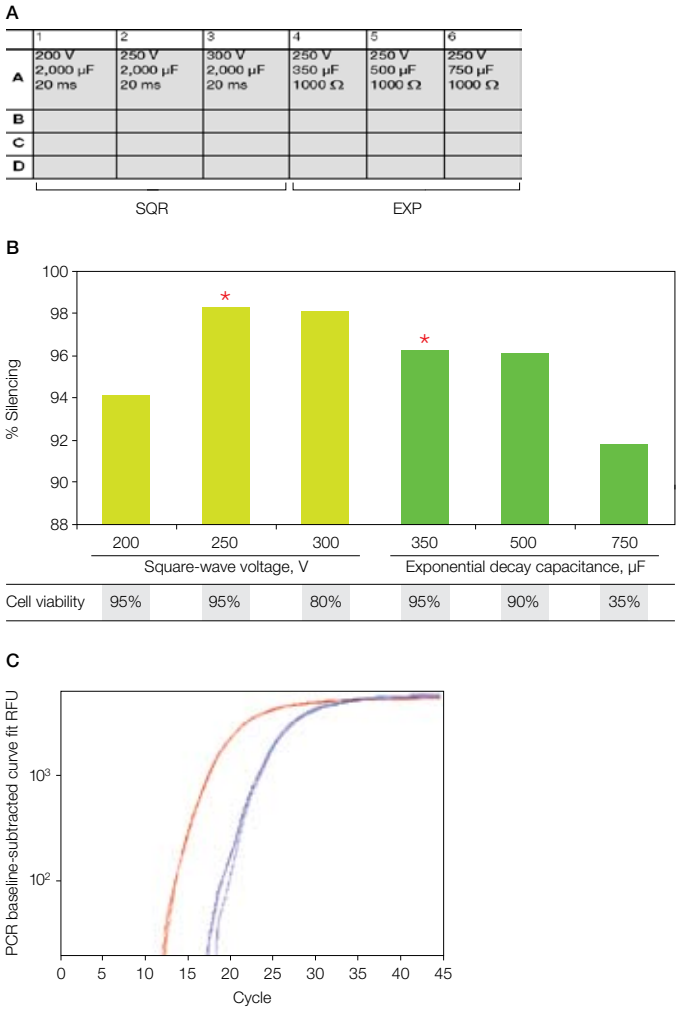

Fig. 2. Preset protocol for siRNA delivery into HeLa cells. A, schematic of the partial-plate preset protocol Opt mini 96-well/Exp, Sqr used in the experiment showing the electroporation parameters and well sets used. Conditions shown in row A are applied to all 4 wells in the column; **B**, percentage of GAPDH silencing, which is calculated by comparing GAPDH expression levels in cells electroporated with the negative control to that of cells electroporated with siRNA targeting GAPDH. The best conditions for the square-wave and exponential decay protocols are indicated by asterisks; **C**, qPCR traces from knockdown experiments. GAPDH (—) and negative control (—) qPCR traces from the best square-wave protocol (250 V, 2,000 µF, 20 ms). Associated table shows resulting cell viability for each change in condition. RFU, relative fluorescent units.

Plasmid Delivery Into HeLa Cells

To find the best electroporation conditions for plasmid delivery into HeLa cells, the preset protocol Opt 24-well/Exp, Sqr (Figure 3A) was applied using a 24-well electroporation plate. This protocol delivers either a voltage or capacitance gradient with an exponential waveform to the top half of the plate, and either a voltage or duration gradient to the bottom half of the plate using a square-wave protocol. Transfection efficiency, indicated by relative light unit (RLU) values, was double in the exponential-decay protocol compared to the square-wave protocol (Figure 3B, C). Cell density was also higher for the exponential-decay than for the square-wave protocols 24 hr after electroporation. Together, these results indicate that the better protocol for electroporating HeLa cells with this plasmid DNA is an exponential-decay waveform (200 V and 350 µF or 250 V and 200 µF).

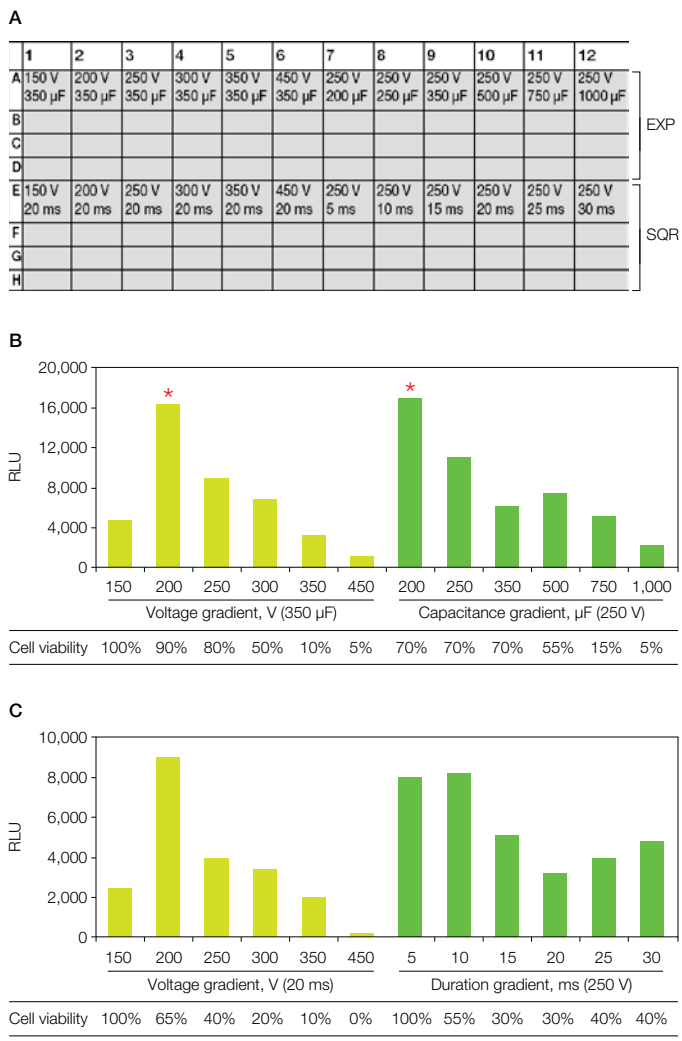

Fig. 3. Optimization of plasmid electroporation in HeLa cells in a 24-well format. A, schematic of the preset protocol Opt 24-well/Exp, Sqr used in the experiment showing the exponential-decay electroporation parameters for each column in rows A–D and square-wave parameters for each column in rows E–H; **B**, results from the preset exponential decay protocol, which allows for a voltage gradient (■) and a capacitance gradient (■); **C**, results for the square-wave protocol, which allows for a voltage gradient (■) and a pulse duration gradient (■). Optimal electroporation conditions (**B**) are marked by asterisks. Associated tables show resulting cell viability for each change in condition. RFU, relative fluorescent units.

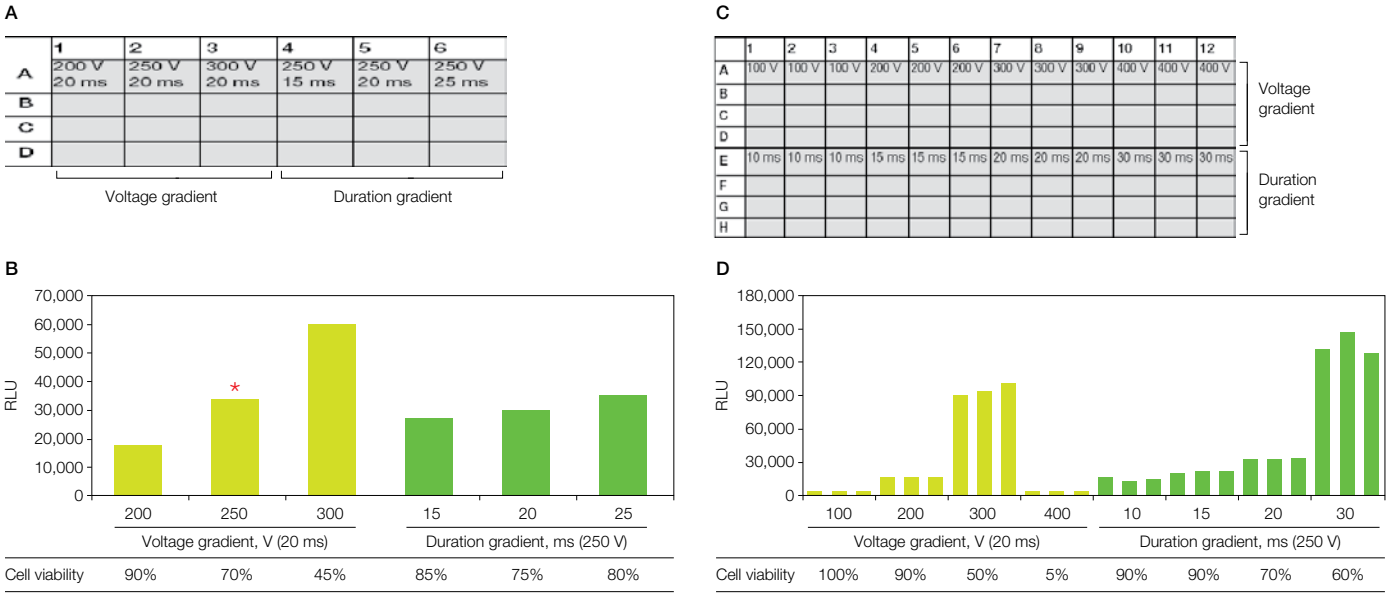

Fig. 4. Optimization of plasmid electroporation in CHO cells. A schematic of the preset protocol used in each experiment is shown above the results chart. The partial-plate preset protocol Opt mini 96-well/Sqr (**A**) and whole-plate protocol Opt 96-well/Sqr, NP, D (**C**) were performed on 96-well electroporation plates. The optimal electroporation conditions are defined by the highest RLU values and the highest cell densities (marked by an asterisk) (**B**, **D**). Associated tables show resulting cell viability for each change in condition.

Plasmid Delivery in CHO Cells

Previous electroporation conditions in the Gene Pulser Xcell™ single cuvette system, indicated that the highest transfection efficiency for CHO cells is obtained using square-wave protocols. In the following experiments, different preset square-wave protocols were applied to CHO cells to determine the optimal electroporation conditions for plasmid delivery in CHO cells. The preset protocol Opt mini 96-well/Sqr (Figure 4A) was applied first. This protocol applies a square wave and generates either a voltage or duration gradient for six well sets. Although 300 V yielded the highest luciferase activity, cell viability was only 45%. Lower voltage conditions (250 V) resulted in greater cell viability, but lower luciferase activity.

A final experiment in which voltage and duration were varied was performed in a 96-well plate (Figure 4C). The results from this experiment further verified those already obtained. The optimal voltage was 250 V and duration was 20–30 msec.

Conclusions

Preset protocols on the Gene Pulser MXcell electroporation system allow rapid, thorough optimization of electroporation parameters to improve transfection efficiency of siRNA and plasmid DNA in mammalian cells. Preset protocols were created to allow many factors that affect electroporation to be tested simultaneously. The data shown exemplifies how preset protocols can be used for optimizing electroporation conditions for the mammalian cell line of interest. Both mini- and whole-plate preset protocols utilizing 96- or 24-well electroporation plate formats were used to electroporate siRNA targeting human GAPDH into HeLa, plasmid (pCMV-iLuc), or CHO cells using exponential-decay or square-wave pulses. The data also demonstrate the benefits of fine-tuning or optimizing transfection experiments, which results in significantly greater transfection efficiency and cell viability.

For additional copies of this article, request bulletin 5687.

Effect of PMA on Phosphorylation of Cx43: A Quantitative Evaluation Using Blotting With Multiplex Fluorescent Detection

Lily Woo,[1] Kevin McDonald,[1] Marina Pekelis,[1] James Smyth,[2] and Robin Shaw,[2]
[1] Bio-Rad Laboratories, Inc., Hercules, CA 94547 USA,
[2] University of California, San Francisco, Cardiovascular Research Institute, San Francisco, CA 94143 USA

Introduction

Cardiac action potentials are normally transmitted through intercellular gap junctions, which consist primarily of the phosphoprotein connexin 43 (Cx43). Cx43 has a relatively short half-life of less than 3 hours, which facilitates rapid changes in cell-to-cell coupling in response to various stimuli (Beardslee et al. 1998). Downregulation of myocardial Cx43 is observed following ischemia, resulting in reduced dissemination of potentially harmful factors via gap junctions (Saffitz et al. 2007). Protein kinase C (PKC) is a well-documented stress sensor, and PKC-mediated phosphorylation of Cx43 reduces gap junction permeability and flags the Cx43 molecule for internalization and degradation following ischemia (Girao and Pereira 2003, Laird 2005, Lampe et al. 2000). Phorbol 12-myristate 13-acetate (PMA) is a potent activator of PKC and is utilized in this study to simulate a stress response and induce phosphorylation of Cx43 in the murine cardiomyocyte cell line HL-1 (Claycomb et al. 1998, Liu and Heckman 1998). The phosphorylation status of Cx43 at serine 368 (Ser^{368}) as a response to PMA treatment was evaluated.

In this study, changes in Cx43 levels and phosphorylation were quantitatively evaluated using western blotting methodology with fluorescent detection. Data demonstrate the ability to detect both protein standards and sample proteins on a blot in a single image capture session using fluorescent signals from multiple color channels. This fluorescent multicolor imaging approach provides a simplified and robust western blotting workflow that allows a shorter protein detection process and results in high-quality quantitative data, including molecular weight (MW) estimation of sample proteins directly from a blot.

Methods

HL-1 cells were maintained in Claycomb medium (Sigma-Aldrich Co.), supplemented with 10% fetal bovine serum (Invitrogen Corporation), 100 U/ml penicillin, 100 µg/ml streptomycin (Invitrogen), 0.1 mM norepinephrine (Sigma-Aldrich), and 2 mM L-glutamine (Invitrogen), and maintained at 37°C, 5% CO_2, 95% air. Cells were cultured in 100 mm cell culture dishes (Corning, Inc.), coated with gelatin and fibronectin (Sigma-Aldrich). Confluent monolayers of cells were treated with 1 µM PMA (Sigma-Aldrich) for 15, 30, 45, and 60 min. Control cells were treated with vehicle (DMSO, Fisher Scientific) for 60 min, and cells were sampled at the end of each treatment, starting from time 0. During sampling, cells were washed with 5 ml Dulbecco's phosphate buffered saline (PBS) (Invitrogen) on ice, lysed in 150 µl RIPA lysis buffer, scraped, and transferred to Eppendorf tubes. Lysates were sonicated and centrifuged at 13,000 rpm at 4°C. Protein concentrations were determined using the *DC*™ protein assay.

Proteins were resolved at a concentration of 30 µg/well using SDS-PAGE and transferred to FluoroTrans PVDF low-fluorescence membranes (Pall Corporation). Membranes were rinsed in TNT buffer twice, blocked for 1 hr at room temperature (RT) in TNT buffer containing 5% nonfat dried milk, washed twice in TNT, and incubated overnight at 4°C with rabbit anti-phospho Cx43 Ser^{368} (Cell Signaling Technology, Inc.; 1:500 in TNT containing 5% BSA). After incubation, membranes were washed 3 x 5 min in TNT to remove unbound antibody and probed with mouse total anti-Cx43 (Sigma-Aldrich; 1:1,000) and rat anti-tubulin (Abcam Inc.; 1:1,000) for 2 hr at RT in TNT buffer containing 5% nonfat dried milk. Unbound antibody was removed by rinsing twice and washing 3 x 5 min in TNT. Membranes were incubated in the dark with secondary antibodies: goat anti-rabbit Alexa Fluor 488, goat anti-rat Alexa Fluor 555, and goat anti-mouse Alexa Fluor 633 (Invitrogen; 1:1,000 in TNT buffer containing 5% nonfat dried milk) for 1 hr at RT. Unbound secondary antibody was removed by washing 4 x 5 min in TNT. Membranes were soaked in 100% methanol for 2 min and allowed to air dry in the dark prior to detection using the Molecular Imager® VersaDoc™ MP 4000 imaging system. Quantitative analyses of blots were performed with Quantity One® 1-D analysis software.

A validation experiment was performed to ensure that data from multiplexed fluorescent western blotting can be quantitated. Two proteins, actin (a housekeeping control protein whose concentration was kept constant) and human transferrin (with varied concentrations), were used for validation. Samples were loaded on a Criterion™ 4–20% gradient Tris-HCl gel, with actin at a concentration of 150 ng/lane and transferrin at 25, 12.5, and 5 ng/lane (n = 3 for each concentration). To determine MW and to assess transfer efficiency, 5 µl of Precision Plus Protein™ WesternC™ standards were run alongside the sample proteins on the gel. Proteins were transferred to FluoroTrans PVDF membrane and blocked with BSA-PBS buffer for 1 hr at RT.

Membrane was then incubated with two primary antibodies: rabbit anti-human transferrin (Dako; 1:1,000) and mouse anti-actin (Sigma-Aldrich; 1:3,000) for 1 hr at RT and washed 3 x 10 min in TBS buffer. The blot was incubated at RT with secondary antibodies — goat anti-rabbit Alexa Fluor 647 and goat anti-mouse Alexa Fluor 568 (Invitrogen; 1:1,000 in blocking buffer) for 1 hr in the dark before being washed in TBS wash buffer 3 x 10 min. The membrane was equilibrated in methanol for 2 min and air dried. Imaging was achieved using a Molecular Imager® PharosFX™ system. Alexa Fluor 568 and standards with MWs of 75, 50, and 25 were detected with a 532 nm laser and a 605 nm bandpass filter. A 635 nm laser and a 695 nm bandpass filter were used to detect Alexa Fluor 647, and standards with MWs of 150, 100, and 37. Images were viewed and analyzed using Quantity One software.

Results

Validation of Quantitative Fluorescent Western Blotting

Precision Plus Protein WesternC standards can be used to estimate MW directly from blots by plotting the log MW of the standard bands against the relative migration distance (R_f) of the standards and sample protein bands (for more information, see bulletin 5576).

Band analysis of actin indicated an apparent MW of 41 and mean trace quantity (intensity x mm) of 2,279 with a standard deviation of 159, giving a coefficient of variation (CV) of 6.98% (Figure 1A, C). Transferrin was detected at an apparent MW of 76. The mean trace quantities of transferrin were 1,253, 570, and 238 for each concentration. The CVs were 3.8%, 4.3%, and 24.7%, respectively (Figure 1B, C). The relative quantities of the transferrin loads were 1, 0.5, and 0.2, and the relative calculated quantities after western blotting were 1, 0.45, and 0.19. Data for this analysis are shown in Table 1.

Table 1. Quantitative analysis of fluorescent blotting.

		Transferrin, ng/lane		
	Actin, 150 ng/lane	25	12.5	5
Mean trace quantity	2,279	1,253	570	238
Standard deviation	159.1	47.4	24.4	58.7
CV, %	7.0	3.8	4.3	24.7

Effect of PMA on Phosphorylation Status of Cx43

An increase in phospho Cx43 Ser^{368} (green) was detected at 15 min postincubation with 1 µM PMA (Figure 2A, D). This induction of Cx43 phosphorylation was followed by a reduction in total Cx43 levels (red) at 30 min (Figure 2B, D), consistent with the model of PKC regulation of Cx43 degradation through phosphorylation at Ser^{368}. Quantitative results were normalized to tubulin (purple), which served as an internal control (Figure 2C, D). Phosphorylation of Cx43 was sustained for the duration of the experiment, relative to the total levels of Cx43, which remained significantly reduced (Figure 2E).

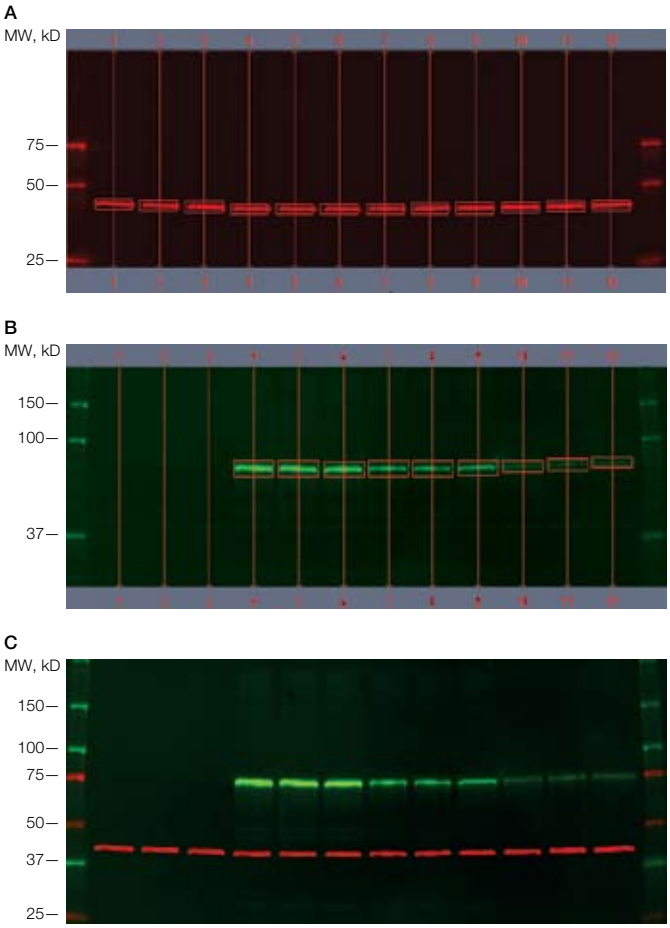

Fig. 1. Validation of quantitative fluorescent blotting. A, fluorescent image of blot probed with anti-actin; all lanes had equal protein loads (150 ng/lane); **B**, fluorescent image of blot probed with anti-human transferrin; amount of protein/lane varied (lanes 1–3, 0 ng; lanes 4–6, 25 ng; lanes 7–9, 12.5 ng; lanes 10–12, 5 ng); **C**, merged image of A and B.

Conclusions

The loss of gap junctional intercellular communication as a result of altered expression/localization of Cx43 seriously impacts the function of the working myocardium in ischemic heart disease. Despite protective effects elicited by the body to contain the spread of potentially toxic factors, uncoupling of gap junctions prevents cardiomyocytes from contracting in a coordinated manner and can lead to pathologies, such as ventricular fibrillation. In this study, we illustrate that exposure of a cardiomyocyte cell line (HL-1) to PMA results in the rapid PKC-mediated phosphorylation of Cx43 at Ser^{368}. It is believed that phosphorylation of Cx43 not only reduces gap junction permeability, but also promotes internalization and degradation of the Cx43 protein. Consistent with this model, we observed a significant reduction in total Cx43 levels following induction of PKC-mediated phosphorylation at Ser^{368}, similar to that observed in ischemic heart disease. The function of cardiac PKC is being elucidated further and is emerging as an attractive candidate for therapeutic intervention in ischemic heart disease.

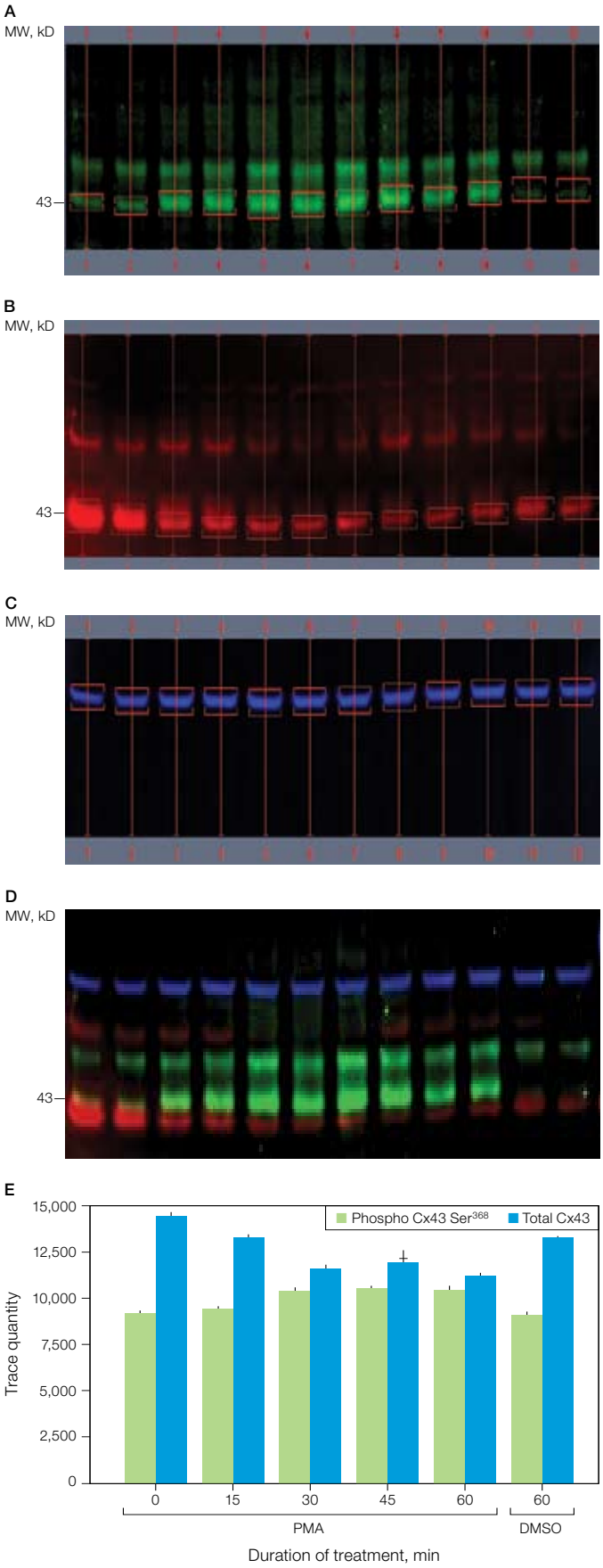

Table 2. Duration of drug treatment of HL-1 cells.

Lanes	Duration, min	Drug
1–2	0	PMA
3–4	15	PMA
5–6	30	PMA
7–8	45	PMA
9–10	60	PMA
11–12	60	DMSO

We also investigated the practicality of fluorescent western blotting for multiplexing protein detection and demonstrated the method of quantitation using proteins of known concentrations. In addition, the use of high-quality MW standards such as Precision Plus Protein WesternC standards allows simultaneous estimation of sample protein MW directly from blots without additional steps. With multiplex blotting, a control "housekeeping" protein can be used as a loading reference and correction factor for more accurate quantitation of a second protein of interest, which may have varying levels of expression.

References

Beardslee MA et al., Rapid turnover of connexin43 in the adult rat heart, Circ Res 83, 629–635 (1998)

Claycomb WC et al., HL-1 cells: a cardiac muscle cell line that contracts and retains phenotypic characteristics of the adult cardiomyocyte, Proc Natl Acad Sci USA 95, 2979–2984 (1998)

Girao H and Pereira P, Phosphorylation of connexin 43 acts as a stimuli for proteasome-dependent degradation of the protein in lens epithelial cells, Mol Vis 9, 24–30 (2003)

Laird DW, Connexin phosphorylation as a regulatory event linked to gap junction internalization and degradation, Biochim Biophys Acta 1711, 172–182 (2005)

Lampe PD et al., Phosphorylation of connexin43 on serine368 by protein kinase C regulates gap junctional communication, J Cell Biol 149, 1503–1512 (2000)

Liu WS and Heckman CA, The sevenfold way of PKC regulation, Cell Signal 10, 529–542 (1998)

Saffitz JE et al., Remodeling of gap junctions in ischemic and nonischemic forms of heart disease, J Membr Biol 218, 65–71 (2007)

For additional copies of this article, request bulletin 5685.

Fig. 2. Effect of 1 µM PMA on phosphorylation of Cx43 in the cardiomyocyte cell line HL-1. A, phosphorylated Cx43; **B**, total Cx43; **C**, tubulin; **D**, merged images of A, B, and C; and **E**, plot of trace quantity from blot probed for phospho Cx43 and total Cx43 against duration of drug treatment. Duration of treatment is described in Table 2.

Applications of the ProteOn™ GLH Sensor Chip: Interactions Between Proteins and Small Molecules

Boaz Turner, Moran Tabul, and Shai Nimri, Bio-Rad Laboratories, Inc., Gutwirth Park, Technion, Haifa, 32000, Israel

Introduction

The ProteOn GLH sensor chip is one of several types of sensor chips available for use with the ProteOn™ XPR36 protein interaction array system (Figure 1). The chip is designed for protein-small molecule and protein-protein interaction studies in which highest sensitivity is of primary concern.

The GLH sensor chip, similar to other general amine coupling ProteOn sensor chips (GLC and GLM), utilizes a proprietary surface chemistry enabling easy activation of carboxylic groups by *N*-hydroxysulfosuccinimide (sulfo-NHS). This activation provides efficient binding of proteins via their amine groups, and ensures high ligand activity in many biological applications (see bulletin 5404).

Of the ProteOn sensor chips, the GLH chip offers the highest ligand binding capacity, making it optimal for the study of protein-small molecule interactions. This higher capacity is attained through the structure of its surface binding layer, comprising a unique formula of modified polysaccharides. Higher binding capacity, together with efficient preservation of the protein's biological activity, ensures high analytical response upon binding of the analyte to the ligand — a key advantage when measuring the response of small molecule compounds.

In this report, we describe the use of the ProteOn GLH sensor chip with the ProteOn XPR36 system. To demonstrate the high binding capacity and the versatility of the GLH chip, immobilization levels of 11 different proteins with a wide range of isoelectric point (pI) values were evaluated. In addition, to demonstrate the efficient binding properties and exceptionally high ligand activity, interaction studies between proteins and small molecules (MW <1,000) were illustrated by two biological models: 1) carbonic anhydrase II (CAII) and small molecule inhibitors, and 2) a monoclonal antibody specific to the dinitrophenyl (DNP) group and dinitrophenyl-labeled amino acids.

CAII Small Molecule Inhibitors

The family of CA proteins is a group of metalloenzymes that catalyze the conversion of carbon dioxide to bicarbonate and protons. Some CA inhibitors are active ingredients in drugs that treat diseases such as glaucoma or epilepsy. Kinetic studies of the interaction between CAII and its inhibitors appear in the literature (for example, Myszka 2004, Myszka et al. 2003). The interaction of CAII with ten different inhibitors was studied with the ProteOn GLH sensor chip, showing high analytical response in comparison to published data using conventional chip surfaces.

Additionally, the high ligand activity and analytical response were further demonstrated by a multichip study of the interaction of CAII with one of its inhibitors, 4-carboxybenzenesulfonamide (CBS). CAII was immobilized at different ligand densities and reacted with six concentrations of CBS. Analysis of the results revealed that CAII ligand activity was more than 80% and thus yielded exceptionally high analyte signals.

A Monoclonal Antibody Specific to the DNP Group and Three Types of DNP-Labeled Amino Acids

The labeling of peptides, proteins, and other biomolecules with DNP groups and the use of antibodies to bind DNP is a widely used detection method in research and diagnostic applications;

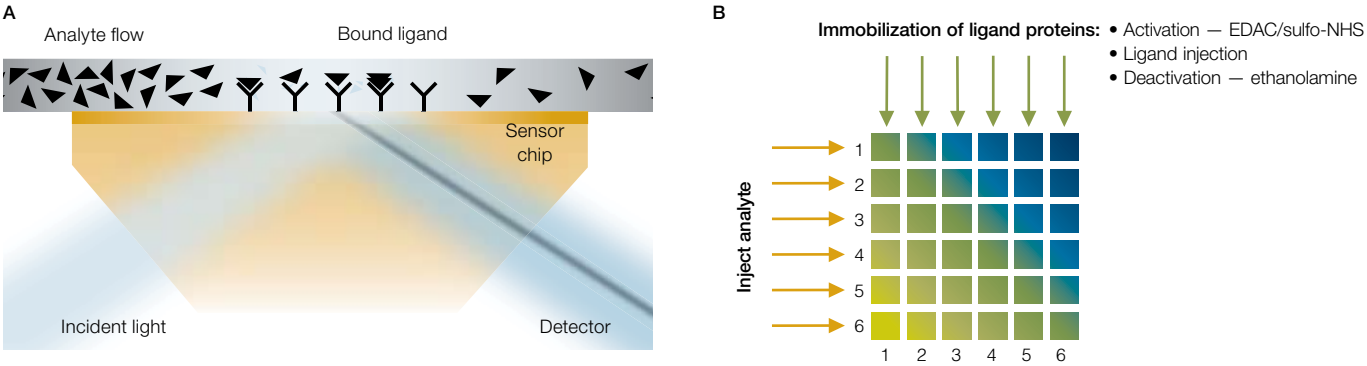

Fig. 1. Schematic illustration of ProteOn XPR36 protein interaction array system technology. A, detection of ligand to analyte interaction; **B**, general experimental procedure for the parallel and simultaneous immobilization of up to six ligand proteins on the sensor chip and the simultaneous flow of small molecules as analytes for the protein-small molecule kinetic studies. EDAC, 1-ethyl-3-(3-dimethylaminopropyl) carbodiimide hydrochloride.

for example, using immunoperoxidase (Jasani et al. 1992). This biological model was chosen to illustrate the ability of the GLH chip to measure the binding of small analytes to large proteins such as antibodies.

Methods

Instrument and Reagents

Experiments were performed using the ProteOn XPR36 protein interaction array system with ProteOn GLH sensor chips. ProteOn PBS/Tween running buffer (phosphate buffered saline, pH 7.4 with 0.005% Tween 20) was used. In certain cases, 3% or 10% dimethyl sulfoxide was added to enable dissolution of the organic analytes. For immobilization of proteins, ProteOn reagents and buffers were used as described in Bronner et al. 2006. The ProteOn amine coupling reagents were EDAC, sulfo-NHS, and 1 M ethanolamine hydrochloride solution, pH 8.5. The ProteOn immobilization buffers were 10 mM sodium acetate solutions, pH 4.0, 4.5, 5.0, or 5.5; manual pH adjustment with 1 M HCl or NaOH was used to generate other pH values. All proteins and small molecule analytes were purchased from Sigma-Aldrich Co. All experiments were performed at 25°C. For details on further assay conditions, see bulletin 5679.

Sensorgram Acquisition and Data Analysis

In each of the kinetic studies, the interactions of six analyte concentrations with up to five immobilized ligands and one reference protein were monitored in parallel. The data were analyzed with ProteOn Manager™ 2.0 software.

Values derived from the spots containing immobilized reference protein (rabbit IgG) were used for reference subtraction. Although the ProteOn XPR36 system enables the use of unmodified spots or interspots as references, it is recommended in cases of very high ligand density to use spots with a reference protein, where the conditions are more similar to the active spots.

Each set of six reference-subtracted sensorgrams was fitted globally to curves describing a homogeneous 1:1 biomolecular reaction model. Global kinetic rate constants (k_a and k_d) were derived for each reaction, and the equilibrium dissociation constant, K_D, was calculated using the equation $K_D = k_d / k_a$. The R_{max} values, the maximal analyte signals at saturation of the active binding sites of the ligand, were also calculated from this analysis.

Determination of K_D in the CAII/methylsulfonamide interaction was done by measurement of the equilibrium response for each of the six analyte concentrations. These equilibrium response levels (R_{eq}) were then fitted to a simple bimolecular equilibrium model at 50% saturation response.

Results and Discussion

Immobilization of Proteins With Different pI Values

Proteins with various pI values were immobilized onto the ProteOn GLH chips. The results are illustrated in Figure 2 and summarized in Table 1. Figure 2 compares the immobilization levels of the GLH chip to the ProteOn GLM chip, and to published results for a series of proteins immobilized under similar conditions (Johnsson et al. 1991). The GLH chip, used with sulfo-NHS activation, is capable of immobilizing high levels of proteins with a wide range of pI values. Effective binding of even very-low pI proteins such as pepsin, which is difficult with other methods as reported in the literature, is possible with the GLH sensor chip.

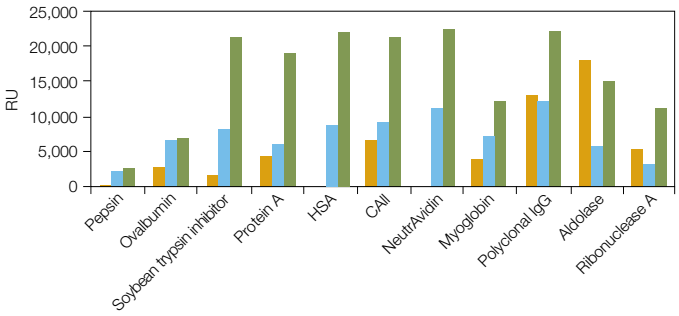

Fig. 2. Comparison of ligand immobilization levels for various proteins between previously published values using conventional surface (■) chips, and results obtained on GLM (■) and GLH (■) chips. Data for conventional surfaces with HSA and NeutrAvidin were not reported in the literature. RU, response units.

Table 1. Results of immobilization of 12 proteins with various pI values onto ProteOn GLH chips.

Protein	pI	MW	Immobilization Conditions*	Final Amount of Bound Ligand, RU
Pepsin	3.0	34,700	800 µg/ml, pH 2.7	2,470
Ovalbumin	4.5	43,500	400 µg/ml, pH 4.0	6,800
Soybean trypsin inhibitor	4.5	20,000	400 µg/ml, pH 4.0	21,200
Protein A	5.1	41,000	300 µg/ml, pH 4.5	18,800
Human serum albumin (HSA)	5.1	66,000	50 µg/ml, pH 5.0	22,000
Carbonic anhydrase II	5.9	29,000	125 µg/ml, pH 5.0	21,200
NeutrAvidin	6.3	60,000	50 µg/ml, pH 4.5	22,350
Myoglobin	6.9–7.4	17,000	400 µg/ml, pH 6.0	12,200
Polyclonal rabbit IgG	6.0–8.0	150,000	25 µg/ml, pH 5.0	22,200
Aldolase	8.2–8.6	161,000	100 µg/ml, pH 6.0	14,850
Ribonuclease A	9.3	13,700	400 µg/ml, pH 6.0	11,300

* In 10 mM sodium acetate solution at the indicated pH.

CAII Small Molecule Inhibitors

CAII protein was immobilized at a level of 20,000 RU, and the binding of ten small molecule inhibitors was studied. The data for the kinetic analysis are shown in Figure 3, and the results are summarized in Table 2. While the k_a and k_d values are in agreement with data published in the literature, the maximal analytical response was found to be at least four times higher in all cases than shown in similar studies with a conventional sensor chip (Myszka 2004).

Table 2. Results of the interactions of CAII (MW 29 kD) with ten different inhibitors.

Analyte	MW	Highest Concentration Used, µM	k_a, $M^{-1}sec^{-1}$	k_d, sec^{-1}	K_D, M	R_{max}, RU
Sulpiride	341	250	2.52×10^3	2.62E-01	1.04E-04	188
Sulfanilamide	172	50	2.40×10^4	1.15E-01	4.79E-06	112
Furosemide	331	50	5.15×10^4	3.66E-02	7.10E-07	180
CBS	201	50	2.83×10^4	3.34E-02	1.18E-06	105
Dansylamide	250	10	1.33×10^5	8.67E-02	6.52E-07	105
1,3-Benzene-disulfonamide	236	10	1.11×10^5	8.96E-02	8.07E-07	99
Benzenesulfonamide	157	50	1.17×10^5	1.18E-01	1.01E-06	114
7-Fluoro-2,1, 3-benzoxadiazole-4-sulfonamide	217	2	4.64×10^5	1.32E-02	2.84E-08	82
Acetazolamide	222	2	9.28×10^5	2.43E-02	2.62E-08	99
Methylsulfonamide	95	2,500	—	—	3.15E-04	22

Monoclonal Antibody and DNP-Labeled Amino Acids

The binding of three DNP-labeled amino acids (DNP-glycine, DNP-valine, and DNP-tryptophan) was studied to illustrate the ability of the ProteOn GLH sensor chip to measure the binding of small analytes to large ligands (Table 3, Figure 4). The amount of immobilized anti-DNP was 18,550 RU. Greater than 50% of the total binding sites were active. In the case of DNP-glycine, the molecular weight ratio of ligand to analyte is greater than 300 (assuming two available ligand binding sites per ligand molecule), and binding of such analytes is readily detected and measured.

Table 3. Results of the interactions of monoclonal anti-DNP (150 kD) with three DNP-labeled amino acids.

Analyte	MW	k_a, $M^{-1}sec^{-1}$	k_d, sec^{-1}	K_D, M	R_{max}, RU
DNP-glycine	241	1.99E+06	0.095	4.77×10^{-8}	36
DNP-valine	283	1.24E+06	0.098	7.90×10^{-8}	41
DNP-tryptophan	370	7.14E+05	0.251	3.52×10^{-7}	75

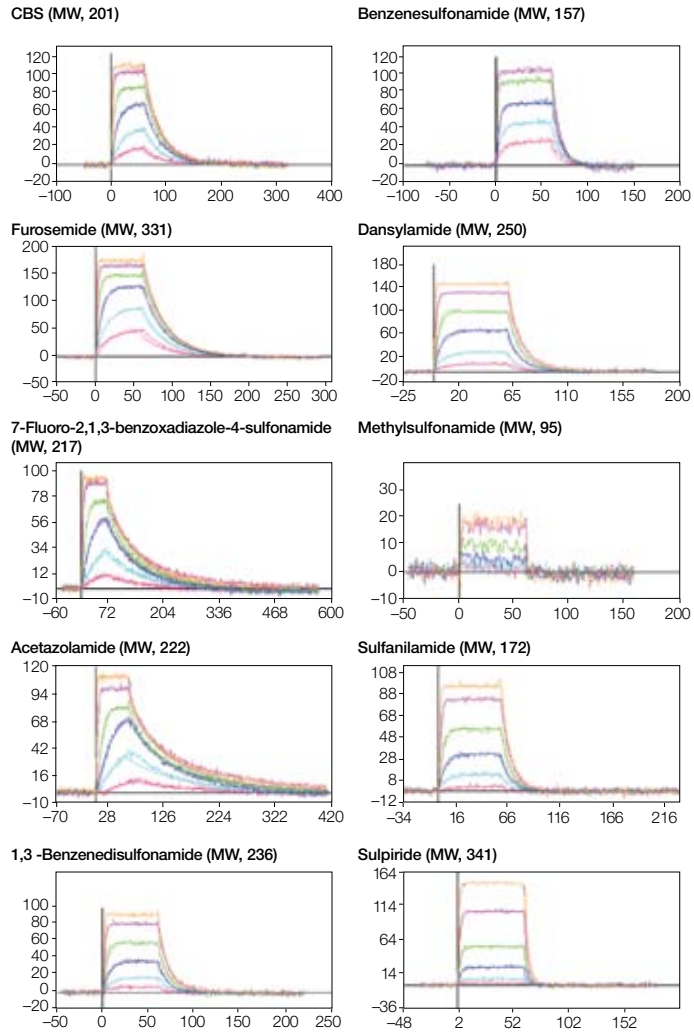

Fig. 3. Sensorgrams and analysis fit from each of the kinetic studies of CAII (20,000 RU) and the pertinent inhibitor. The kinetic parameters are shown in Table 2.

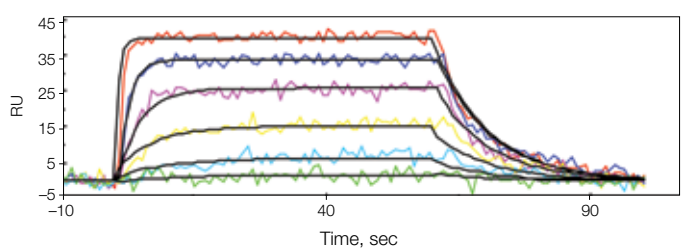

Fig. 4. Sensorgrams and analysis fit from the kinetic study of anti-DNP (18,550 RU) and the DNP-valine analyte. The kinetic parameters are shown in Table 3.

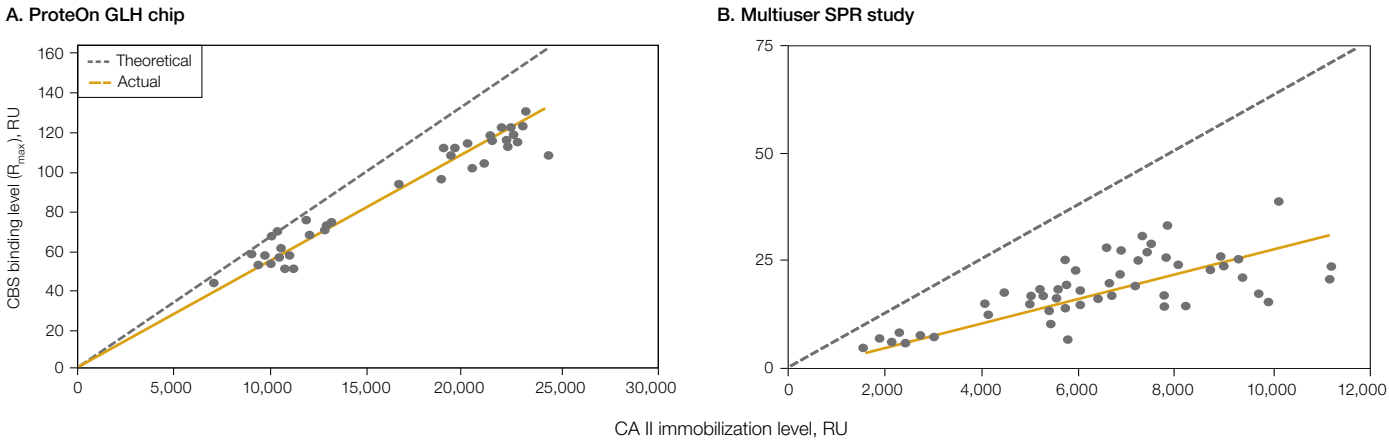

Fig. 5. Analytical response of CBS binding versus the amount of CAII immobilized onto the sensor chip. A, ProteOn GLH chip; **B**, conventional chip (Myszka et al. 2003). The black dotted line shows the theoretical maximal response, assuming that 100% of the bound ligand molecules are active. The gold line is a linear fit of the actual response values. Actual ligand activity is 82% of theoretical for the GLH chip and 46% for the conventional chip surfaces.

Multichip Study of the CAII/CBS Interaction

The bound amount of the CAII ligand ranged from 7,000 to more than 24,000 RU, depending on the level of surface activation. The kinetic analysis of the interaction with CBS was performed for each of the 35 sets of results; each set contained six analyte sensorgrams relating to one ligand density. The average results of kinetic constants were: $k_a = 3.2 \pm 0.7 \times 10^4$ $M^{-1}sec^{-1}$; $k_d = 0.037 \pm 0.003$ sec^{-1}; $K_D = 1.2 \times 10^{-6} \pm 0.3 \times 10^{-6}$ M. These values are in agreement with published data (Myszka et al. 2003).

The mean ligand activity of the CAII was determined by plotting the maximal response of the analyte (R_{max}) versus the ligand density (Figure 5A). Assuming a stoichiometric relationship between reactants in molar terms, the theoretical CBS binding response is 150-fold lower than the immobilized level of CAII due to the mass difference between the interacting pair. The dotted trend line in Figure 5A represents the theoretical correlation between the surface density of CAII and maximal binding signal of CBS. Experimental data typically falls below this line because some of the immobilized protein is inactive. However, the data for the ProteOn GLH chip (Figure 5A) shows that actual CBS binding values lie very close to the theoretical trend line, indicating that more than 80% of the immobilized ligand is active. These results demonstrate exceptionally high ligand activity of the CAII/CBS interaction, and are a significant improvement over the reported literature results of less than 50% ligand activity (Figure 5B, from Myszka et al. 2003). In absolute terms, analyte signals of more than 120 RU could be gained with the GLH chip, while less than 40 RU was the maximal value recorded with conventional surfaces.

Conclusions

The ProteOn GLH sensor chip offers exceptionally high binding capacities while preserving ligand activity, providing enhanced analyte signal in situations where the molecular weight ratio of ligand to analyte is very high (~100 or more). These advantages make the GLH chip an ideal choice for protein-small molecule and protein-protein interaction studies where highest sensitivity is desired. Used with the ProteOn XPR36 protein interaction array system, up to 36 biomolecular interactions can be assayed simultaneously in one experiment, yielding valuable kinetic, concentration, and equilibrium data, and reducing research time from days to hours. The GLH chip is a valuable tool for the lead identification and optimization processes of drug development, as well as areas of fundamental research in protein-small molecule interactions and developmental work in assay optimization.

References

Bronner V et al., Rapid optimization of immobilization and binding conditions for kinetic analysis of protein-protein interactions using the ProteOn XPR36 protein interaction array system, Bio-Rad bulletin 5367 (2006)

Jasani B et al., Dinitrophenyl (DNP) hapten sandwich staining (DHSS) procedure. A 10 year review of its principal reagents and applications, J Immunol Methods 150,193–198 (1992)

Johnsson B et al., Immobilization of proteins to a carboxymethyldextran-modified gold surface for biospecific interaction analysis in surface plasmon resonance sensors, Anal Biochem 198, 268–277 (1991)

Myszka DG, Analysis of small-molecule interactions using Biacore S51 technology, Anal Biochem 329, 316–323 (2004)

Myszka DG et al., The ABRF-MIRG'02 study: assembly state, thermodynamic, and kinetic analysis of an enzyme/inhibitor interaction, J Biomol Tech 14, 247–269 (2003)

For an expanded version of this article, request bulletin 5679.

Sample Preparation

5635 ProteoMiner™ system brochure

5632 Accessing low-abundance proteins in serum and plasma with a novel, simple enrichment and depletion method

Chromatography

5668 Profinity eXact™ system brochure

5667 CHT™ ceramic hydroxyapatite product information sheet

5656 Purification of tag-free recombinant proteins using the Profinity eXact fusion-tag system

5655 Profinity eXact purification resin product information sheet

5652 Profinity eXact fusion-tag system, performs on-column cleavage and yields pure native protein from lysate in less than an hour

5646 Profinity eXact cloning and expression kits product information sheet

5591 Profinia™ system installation quick guide

5584 Bio-Scale™ Mini cartridges protein purification product information sheet

Process Chromatography

5665 Bio-Rad® EasyPack™ columns product information sheet

5663 Bio-Rad® InPlace™ columns product information sheet

5661 Media transfer device product information sheet

5659 MainFrame™ lifting accessory product information sheet

5657 SKIDS product information sheet

5644 MacroPrep® High Q product information sheet

5643 MacroPrep® High S product information sheet

5620 Media slurry tank product information sheet (PDF only)

5619 Pressure relief valve product information sheet (PDF only)

5618 Pressure gauge product information sheet (PDF only)

5617 Packing motor product information sheet (PDF only)

5616 Liquid pump for inflatable seals product information sheet (PDF only)

5615 Isolation two-way valves product information sheet (PDF only)

5614 Bubble trap product information sheet (PDF only)

Imaging Systems

5685 Effect of PMA on phosphorylation of Cx43

5609 VersaDoc™ MP imaging system product information sheet

Protein Interaction Analysis

5679 Applications of the ProteOn™ GLH sensor chip

Surface-Enhanced Laser Desorption Ionization (SELDI) Technology

5677 ProteinChip® SELDI system qualification and calibration kits flier

5642 SELDI study and experimental design guide

5602 ProteinChip SELDI system qualification and calibration kits product information sheet

Multiplex Suspension Array Technology

5653 Bio-Plex Pro™ angiogenesis assay panel product information sheet

5651 Bio-Plex Pro human diabetes assay panel product information sheet

5650 Bio-Plex Pro human acute phase assay panel product information sheet

5654 Profiling of human angiogenesis biomarkers in sera of cancer patients using the Bio-Plex® suspension array system (PDF only)

5649 Development and validation of a novel multiplex immunoglobulin isotyping assay on magnetic microspheres

5629 Bio-Plex® Precision Pro™ human cytokine assay flier

5613 Bio-Plex Manager™ software brochure

Microplate Systems

5676 Microplate reader: liquid handling/consumables folder insert

5671 xMark™ microplate absorbance spectrophotometer folder insert

5670 iMark™ microplate absorbance reader folder insert

5669 Asorbance microplate systems folder

Microarray Products

5599 Reverse transfection of mammalian cells for functional screening: results from testing the BioOdyssey™ Calligrapher™ miniarrayer

Gene Transfer

5700 Gene Pulser MXcell system optimization tree flier

5687 Simple and rapid optimization of transfections using preset protocols on the Gene Pulser MXcell electroporation system

5641 Gene Pulser MXcell system optimization protocols

5640 Gene Pulser MXcell system preset protocol quick guide

5634 Gene Pulser MXcell system brochure

5622 Optimization of electroporation conditions with the Gene Pulser MXcell™ electroporation system

Amplification/PCR

5692 Real-time qPCR as a tool for evaluating RNAi-mediated gene silencing

5690 CFX Manager™ software, security edition product information sheet

5689 1000-Series thermal cycling platform interactive demo CD

5648 S1000™ thermal cycler flier

5647 C1000™ thermal cycler flier

5595 C1000 thermal cycler specifications sheet

5594 S1000 thermal cycler specifications sheet

5593 iQ5™ optical system software, security edition product information sheet

5592 CFX96™ real-time PCR detection system flier

5583 1000-Series thermal cycling platform brochure

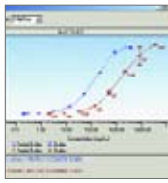

Bio-Plex, Leading Life Science Discovery

Advance your understanding of cell biology and mechanisms of disease with the integrated Bio-Plex system.

Bio-Plex is the most widely cited multiplex assay platform, with research applications in Alzheimer's and Parkinson's diseases, diabetes, obesity, cancer, asthma, cystic fibrosis, autoimmune disease, viral infections, and vaccine development.

The Bio-Plex system enables you to quantitate up to 100 different analytes in one sample with unsurpassed sensitivity, precision, and accuracy, giving you the power to understand complex relationships between proteins in normal and disease states.

For more information, visit us on the Web at
www.bio-rad.com/bio-plex/

Newest Solutions

The following targets are included for each new panel:

Human diabetes 12-plex panel: adiponectin, adipsin, C-peptide, ghrelin, GIP, GLP-1, glucagon, IL-6, insulin, leptin, PAI-1, resistin, TNF-α, visfatin

Human angiogenesis 9-plex panel: angiopoietin-2, follistatin, G-CSF, HGF, IL-8, leptin, PDGF-BB, PECAM-1, VEGF

Human acute-phase 5-plex panel: ferritin, fibrinogen, procalcitonin, serum amyloid A, tissue plasminogen activator

Human acute phase 4-plex panel: α-2-macroglobulin, C-reactive protein, haptoglobin, serum amyloid P

The Bio-Plex suspension array system includes fluorescently labeled microspheres and instrumentation licensed to Bio-Rad Laboratories, Inc. by the Luminex Corporation.

To find your local sales office, visit **www.bio-rad.com/contact/**
In the U.S., call toll free at 1-800-4BIORAD (1-800-424-6723)

Visit us on the Web at **discover.bio-rad.com**

BIO-RAD

WE THINK YOU SHOULD BE ABLE TO OPTIMIZE ON THE FLY

Convenience Is What Happens When You Rethink PCR

Change the way you think about PCR with Bio-Rad's new family of thermal cyclers.

Wouldn't you rather optimize your reactions in minutes and not days? With Bio-Rad's new 1000-series thermal cyclers, optimizing on the fly is just the beginning.

- Easily interchangeable reaction modules meet any experimental or throughput need
- Reduced-mass sample blocks increase ramp rates and reduce run times
- Thermal gradient lets you incubate each row at a different temperature for fast protocol optimization

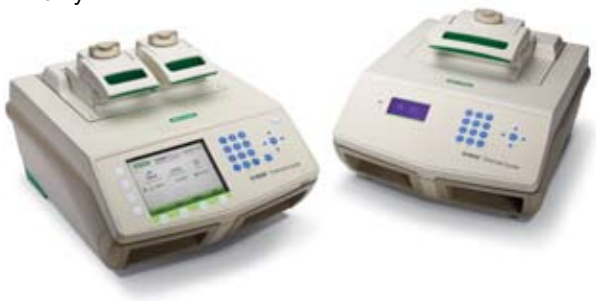

When you rethink PCR, you realize how easy it should be.

For more information, visit us on the Web at **www.bio-rad.com/pcr**

To find your local sales office, visit **www.bio-rad.com/contact/**
In the U.S., call toll free at 1-800-4BIO-RAD (1-800-424-6723)

Visit us on the Web at **discover.bio-rad.com**

BIO-RAD